Revision 1

Helvine-danalite mineralogy of the Dulong Sn-Zn polymetallic deposit in SE Yunnan, SW China

Shiyu Liu[1,2], Yuping Liu[1*], Lin Ye[1*], Chen Wei[1,2], Weihong Chen[1,2]

[1]*State Key Laboratory of Ore Deposit Geochemistry, Institute of Geochemistry, Chinese Academy of Sciences, Guiyang 550081, China*

[2]*University of Chinese Academy of Sciences, Beijing 100049, China*

ABSTRACT

Southeastern (SE) Yunnan is a major Sn polymetallic province of China, with the Dulong large Sn-Zn polymetallic deposit (in the Laojunshan orefield) being one of the most representative deposits. Our recent work had first identified helvine-group minerals in this deposit. These minerals mainly occur in massive sphalerite ores, and coexist with sphalerite, pyrrhotite, biotite, talc, cassiterite, and fluorite. Raman spectroscopic, XRD, SEM, and EPMA analyses indicate that these helvine-group minerals are oscillatory-zoned helvine-danalite. Both the helvine and danalite zones are mixed with varying proportion of the other helvine-group end-member, and our studies indicate that the oscillatory zoning was formed mainly by periodic fluctuations of the fluid physicochemical conditions (notably fS_2 and fO_2), but less related to the variation of the fluid Mn, Fe, and Zn contents. The helvine zone was likely formed in a higher fS_2 but lower fO_2 environment than the danalite zone. In this study, we present the first LA-ICP-MS in-situ trace element data for the helvine-danalite minerals from Dulong, and the results indicate that the helvine has considerably high contents and wider range of trace elements. The helvine is rich in Ca, Al, Sc, and Y, whilst the danalite is rich in Sn and P (reaching thousands of ppm). Such trace element enrichments are likely controlled by their

respective ionic radius and chalcophile behavior.

Meanwhile, the fO_2 and fS_2 conditions during the zoning formation may have also influenced the trace element distributions: trace elements may have mainly entered the helvine-group minerals by substituting into the M-site cations of $M_4[BeSiO_4]_3S$, for instance Al, Sc, and Y substitute for Mn, and Sn, Mg for Fe and Zn. It is noteworthy that the helvine and danalite zones are all HREE-enriched and have distinct negative Eu anomalies. This may be related to the high fluid F-Y-P contents during the mineral formation. High F-Y fluids can readily incorporate HREEs into helvine-group minerals, and phosphates incorporate HREEs more readily in alkali fluids. Europium occurs as Eu^{2+} in the fluid, causing the negative Eu anomalies observed. We have also identified cassiterite grains in the helvine-group minerals and its coexisting sphalerite. U-Pb dating on these cassiterite grains yielded 86.5 ± 1.6 Ma, coeval with the reported sulfide mineralization age. This indicates that both the Be and Sn-Zn polymetallic mineralization occurred in the Cretaceous, and may have been product of the Late Yanshanian Laojunshan magmatic-hydrothermal activity. Considering the close relations with many W(-Be) deposits nearby (e.g. Nanyangtian, Saxi, and Maka), we considered that the Laojunshan orefield has also substantial Be mineralization potential.

Keywords: Helvine-group minerals; physicochemical environment; major and trace element compositions; LA-ICP-MS; cassiterite U-Pb age; Dulong Sn-Zn polymetallic deposits

INTRODUCTION

Beryllium is a lithophile rare metal (Goldschmidt 1932), with its upper crustal abundance (~2.1 ppm) being around 30 times of its abundance in the primitive mantle (~0.07 ppm) (Taylor et al. 1995). Beryllium minerals are commonly found in hydrothermal deposits associated with granitic

pegmatites, skarns, and alkaline and (sub-)volcanic rocks. In nature, Be minerals mainly comprise silicates and aluminosilicates, among which beryl, bertrandite, and helvine-group minerals have industry value (Grew et al. 2014). Helvine-group minerals are important Be minerals, which have the general formula $M_4[BeSiO_4]_3S$ with M = Mn (helvite), Fe (danalite) or Zn (genthelvite). The crystal structure belongs to sodalite-type, in which the [SiO_4] tetrahedron and [BeO_4] tetrahedron are interlinked in four- or six-membered rings in the crystal lattice (Hassan and Grundy 1985; Nimis et al. 1996). It is generally considered that helvine is formed in granites or granitic pegmatites, especially in their intrusive contact zones or endoskarns. Danalite is commonly formed in skarn or contact metamorphism-related deposits and granite or pegmatite. Genthelvite is considered to be the rarest helvine-group minerals, and its presence is only documented in calc-alkaline granites, pegmatite and some contact replacement-type altered rocks (Raade 2020). At present, there are not many studies on the helvine mineralogy in the region, and not much is known for its trace element (including REE) compositions, or any petrogenetic link between the helvine-group minerals.

The Laojunshan region in SE Yunnan is an important Be province in China (Li et al. 2017), which hosts the large Nanyangtian beryl gemstone deposit and the small Saxi beryl gemstone deposit/prospect. In recent years, helvine mineralization was discovered at Maka in the northern part of the Laojunshan intrusion (Du et al. 2014). These deposits/prospects are distributed around the Late Yanshanian Laojunshan intrusion (Fig. 1), but there is basically no research on the Be mineralogy in the area, with the Be mineralization age and ore-formation process still under dispute. The Dulong Sn-Zn polymetallic deposit is the largest (superlarge-scale) polymetallic deposit in the district (Fig. 1), and is widely accepted that its mineralization is closely related to the Laojunshan granite (e.g. Wang et al. 2014; He et al. 2014, 2015; Xu et al. 2015; Ye et al. 2016, 2017, 2018; Zhao

et al. 2018). In this paper, our study has first discovered abundant independent Be minerals (helvine-group) from the deposit. It is note worthy that some of the helvine-group minerals are euhedral and oscillatory zoned, and contain several geochemical indicator elements (e.g. Mn, Fe, Zn) that can provide more information on the SE Yunnan Be ore-formation process and helvine mineralogy. we conducted laser Raman spectroscopy, X-ray diffraction (XRD), back-scattered electron (BSE) imaging, electron probe microanalysis (EPMA), and laser ablation-inductively coupled plasma-mass spectrometry (LA-ICP-MS) analysis on the helvine-group minerals from the Dulong orefield, in order to understand their mineralogy and the physicochemical conditions of the formation of these minerals. We conducted also U-Pb dating on the cassiterite coexisting with Be minerals to unravel the timing of Be mineralization in the Laojunshan orefield.

GEOLOGICAL BACKGROUND

The Dulong ore district is located in the southwestern part of the Laojunshan Metamorphic Core Complex, and situated in tectonic junction between the western end of the Huanan nappes, the Yangtze block, and the Ailaoshan fold belt (Fig. 1a). Exposed stratigraphy in the region comprises mainly the Paleoproterozoic Mengdong Group and Cambrian Xinzhai Formation, Cambrian and Devonian sedimentary rocks, and Silurian Nanwenhe and Cretaceous Laojunshan granites (Fig. 1b). The Paleoproterozoic Mengdong Group is dominated by two-mica (quartz) schist, granulite, and plagioclase amphibolite, which was SHRIMP zircon U-Pb dated to be ca. 761–829 Ma (Liu et al. 2006). The Silurian Nanwenhe granite (SHRIMP zircon U-Pb age: ca. 440–420 Ma; Liu et al. 2006) is exposed in the eastern Dulong, and was metamorphosed/deformed during the Triassic Indosinian orogeny (Yan et al. 2006). The Cretaceous Laojunshan granite is an intrusive complex and

comprises (i) medium- to coarse-grained two-mica monzogranite (100–118 Ma) around (ii) medium- to fine-grained two-mica monzogranite (90–98 Ma). These rocks were intruded by (iii)quartz porphyry and granite porphyry stocks (76–88 Ma) (e.g. Liu et al. 2007; Lan et al. 2016). Previous petrological and geochemical studies indicated that these granite suites are all highly-fractionated S-type, and sourced from partial melting of the Mesoproterozoic argillaceous bedrocks. These magmatic suites were likely formed in a back-/intra-arc extensional environment, associated with large-scale lower crustal delamination and asthenospheric upwelling (e.g. Xu et al. 2015; Zhao et al. 2018). Regional faults at Dulong include mainly the NW-trending Maguan-Doulong and Nanwenhe faults, and a set of NE-trending secondary faults (Fig. 1b).

The Dulong deposit, located on the southern margin of the Laojunshan granite (Fig. 1b), contains five ore blocks: the Tongjie, Manjiazhai, Lazizhai, Nandangchang, and Wukoudong (from north to south) (Fig.1 c). At Dulong, sedimentary rocks are dominated by the Cambrian Xinzhai Formation (main ore host) and Middle Cambrian Tianpeng Formation, which are separated by the NS-trending F_2 fault. The Xinzhai Formation is composed of quartz–mica schist, marble, granulite and minor gneiss. The overlying Tianpeng Formation comprises marble and phyllite, and is exposed only in the western Dulong. Three sets of faults were identified at Dulong: NW-trending Maguan-Dulong fault, NS-trending ore-controlling faults (F_0, F_1 and F_2), and NW-trending strike-slip fault (F_4) (Fig. 1c). The only granitic rocks exposed at the mine are the late quartz porphyry and granite porphyry dike or apophyses, which represent the southernmost extension of the Laojunshan granite. The early-stage two-mica monzogranite was intersected in drill-holes at depth (Su et al. 2016). Recent geological and geochemical studies suggested that the Dulong Sn-Zn polymetallic mineralization was closely related to the Laojunshan granitic magmatism, which is best classified

as magmatic-hydrothermal origin (e.g. Wang et al. 2014; He et al. 2014, 2015; Xu et al. 2015; Ye et al. 2016, 2017, 2018; Zhao et al. 2018).

In the Laojunshan orefield, both the Nanyangtian and Saxi W-Be deposits are located on the eastern side of the Laojunshan granite and share similar ore geological features. The Be mineralization mainly occurred as beryl in the Proterozoic Mengdong Group. gneiss, schist and granulite with plagioclase amphibolite interlayers. The beryl crystals are coarse-grained euhedral, some reaching gemstone quality (Liu et al. 2011). The Maka W(-Be) deposit is located in northern part of the Laojunshan intrusion. The area has different rock types and complex structure, with the Early Paleozoic Maka granitic intrusion being the main magmatic rock type. At Maka, exposed stratigraphy includes mainly the Lower Cambrian Xinzhai Formation and Middle Cambrian Tianpeng Formation, and Be minerals (helvine) coexist with the W mineralization (Du et al. 2014).

SAMPLING AND ANALYTICAL METHODS

Helvine-group samples of this study were collected from the Sn-Zn polymetallic orebody in the Manjiazhai ore block (Fig. 1c). The Be mineral samples were prepared into 200 μm-thick polished thin-sections for the subsequent SEM-BSE and EPMA analyses.

Identification of mineral types and features were mainly performed through laser Raman spectroscopic and scanning electron microscope (SEM) analyses. EPMA major and major element mapping analysis, together with LA-ICP-MS trace element analysis, were carried out. To constrain the Be mineralization age, LA-ICP-MS U-Pb dating was conducted on the cassiterite grains in the helvine minerals and their coexist sphalerite. All these above-mentioned analyses were conducted at the State Key Laboratory of Ore Deposit Geochemistry (SKLODG), Institute of Geochemistry, Chinese Academy of Sciences.

133 **Laser Raman Spectroscopy**

134 The analysis was conducted with a Renishaw in Via^{TM} Reflex confocal laser Raman
135 spectrometer (UK). The analysis used Ar^{+} laser, 532 nm wavelength, 50× magnification, 1 μm laser
136 beam size, 514 nm spectroscopic resolution, and 200–1100 cm^{-1} spectroscopic range.

137 **XRD**

138 The powder XRD analysis used a Empyream XRD diffractometer (Netherland). Experiment
139 setting and conditions include a Cu target, 40 kV voltage, 40 mA current, 15°–95° scan range
140 (2θ), 10(°) /min scan speed, and 0.026° step size.

141 **SEM**

142 The analysis used a JSM-7800F Field Emission SEM (Japan), coupled with a EDAX TEAM
143 Apollo XL Energy Dispersive Spectroscopy (EDS) and the latest TAEM software version (UK).
144 The SEM-EDS can perform fast and accurate qualitative/semi-quantitative determination of mineral
145 phases and their distribution, together with line and planar scanning.

146 **EPMA**

147 The analysis used a JXA8530F-plus Field Emission EPMA (JEOL, Japan). The secondary
148 electron image resolution can reach 3 nm (30 kV, working distance 11 mm), with the spatial
149 resolution better than 0.1 μm. Analytical conditions include 25kV accelerating voltage, 1.0×10^{-8}A
150 current, 10 μm electron beam size. Since there is no corresponding helvine-group mineral standard,
151 we used almandine (to calibrate FeO, MgO), pyrope (to calibrate TiO_2, Cr_2O_3, Al_2O_3), johannsenite
152 (to calibrate MnO, SiO_2), barite (to calibrate SO_3), willemite (to calibrate ZnO) as standards. The
153 lowest detection limit for the elements analyzed is 0.01%, and the relative error is ±2%. Considering
154 that EPMA direct measurement of Be is still technically difficulty (Zhang et al. 2020), the Be

contents in helvine are commonly calculated by assuming the stoichiometric ratios of Be with other elements or element groups. Previous studies suggested various ways of calculation: (1) helvine-group minerals ideal formula $\sum M$: Be = 4:3 calculation (Dunn et al. 1976); (2) 12(Al+Be+Si) calculation (Hassan and Grundy 1985; Ragu et al. 1994); (3) 4(Mn+Fe+Zn) calculation (Langhof et al. 2000); (4) 26 (O+S) calculation (Deer et al. 2004; Zito and Hanson 2017); (5) 3Si and 3Be calculation (Raade 2020). Through detailed comparison analysis of published calculation results, Raade (2020) considered that the assumption of Si = 3 and Be = 3 can effectively avoid the problem of M-site cation substitution by other trace elements in the helvine-group minerals, and yield more accurate and reasonable results. This calculation method, therefore, is used in this study.

LA-ICP-MS trace-element analysis

Trace element analysis used a Coherent 193 nm laser ablation system coupled with an Agilent 7900x ICP-MS. Multiple external standards of USGS reference glass (NIST 610, NIST612, BCR-2G, BIR-1G, BHVO-2G, CGSG-1, analyzed with 44 μm beam size) and no internal standard were used for the calibration and quantitative elemental content calculation (Liu et al. 2008). Recommended elemental contents of the USGS glass are from the GeoReM database (http: //georem.mpch-mainz.gwdg.de/). Offline processing of the obtained data, including sample and blank signal selection, instrumental drift calibration, and elemental contents calculation, were performed with the ICPMSDataCal software (Liu et al. 2010).

LA-ICP-MS U-Pb dating

The analysis used the same equipment as the mineral trace-element analysis. Analysis conditions include 60 μm laser beam size, 4 J/cm^2 energy frequency, 6 Hz repetitive frequency. To

177 increase sensitivity, helium is used as a carrier gas to mix with the Ar make-up gas before entering
178 the ICP. In-house standard AY-4 was used, and the detailed analysis process is as described by Zhang
179 et al. (2017). Offline processing of raw data, and the calculation of U-Th-Pb isotope ratios and age
180 were performed with the ICPMSDataCal software (Liu et al. 2010).
181
182 **RESULTS**
183 **Helvine-danalite assemblage**
184 XRD results are illustrated in Figure 2a, which show that the Be minerals are danalite, and they
185 coexist with minerals such as sphalerite, biotite and pyrrhotite. Raman spectroscopy results show
186 that the Be minerals are helvine (Fig. 2b). It is noteworthy that the three end-member minerals of
187 helvine-group have very similar Raman spectral peaks. As a result, although XRD and Raman
188 analyses can identify helvine-group minerals, they cannot distinguish effectively between the three
189 end-member minerals.
190 In hand-specimen, these helvine-group minerals display triangular profile features. They occur
191 in massive sphalerite ores (Fig. 3-a, b) and coexist with minerals such as sphalerite, pyrrhotite,
192 biotite, and talc (Fig. 3-c, d). Besides, pyrrhotite displays exsolution textures in sphalerite. Under
193 the microscope, it is observed that fine-grained cassiterite coexists with sphalerite and helvine (Fig.
194 3-e, f).
195 In the BSE images, some Be minerals developed clear oscillatory zoning (Fig. 4a), as shown
196 by darker helvine and brighter danalite zones and (from inside out) helvine → danalite alternating
197 growth zones. This shows that these Be minerals are oscillatory-zoned helvine-danalite (Fig. 4 a-b).
198 Fluorite veinlets or grains are commonly found inside the helvine-group minerals, and coexist with

199 sphalerite or pyrrhotite (Fig. 4c). It is noteworthy that the helvine minerals commonly contain some
200 exsolved minerals, including cassiterite, biotite, ilmenite, apatite, (Fig. 4d-f).

201 **Major element compositions of helvine-danalite**

202 Results of the EPMA analysis and major-element 2D scan (Fig. 5) and line scan (Fig. 6c) are
203 given in Table 1. BSE imaging and EPMA results show that the helvine-danalite grains have many
204 zones from core to rim, with each zone having different chemical compositions (mainly in Mn, Fe,
205 and Zn) (Figs. 5, 6a): MnO = 8.38–38.70 wt.%, FeO = 9.91–33.68 wt.%, ZnO = 1.58–9.21 wt.%.
206 In contrast, the Si, S, and **BeO contents have similar ranges: SiO_2 = 32.63–32.89 wt.%, S = 5.71–
207 5.85 wt.%, **BeO = 13.59–13.70 wt.%. Content variations of Mn, Fe, and Zn across adjacent zone
208 are relatively large, and the variation trend for Fe and Zn is the opposite of that for Mn (Fig. 5).
209 Helvine-group minerals include the end-member minerals of helvine ($Mn_4(BeSiO_4)_3S$), danalite
210 ($Fe_4(BeSiO_4)_3S$), and genthelvite ($Zn_4(BeSiO_4)_3S$). From the mineral core to rim, no genthelvite is
211 identified in any zone, and inside the helvine and danalite there is varying amount of the other two
212 end-members (Fig. 6b-c). Geochemically, the Al and Mg contents are relatively low, and they show
213 covariation patterns with Mn, Fe, and Zn (Fig. 6d).

214 **Trace element compositions of helvine-danalite**

215 For the helvine and danalite zones in the helvine-danalite minerals, their representative LA-
216 ICP-MS trace element and REE data are illustrated in Figure 7-8 and Table 2 respectively.
217 Concentrations of some elements (K, Mg, Al, P, Ca, Sc, Y, and Sn) in the helvine-danalite samples
218 are rather high (tens to thousands ppm), whereas those of some other elements (Na, V, Cu, Rb, Sr,
219 Zr, Nb, Ag, In, Cs, and W) range from below the detection limit to several tens of ppm. The helvine
220 zones have relatively high Al (481–1483 ppm), Ca (650–2573 ppm), Sc (82–133 ppm), and Y (566–

1277 ppm), whilst the danalite zones have relatively high Mg (1425–2337 ppm), P (1151–1551 ppm), and Sn (652–1326 ppm). The samples show chondrite-normalized HREE enrichments, distinct negative Eu anomalies, and relatively high Y contents (218–1278 ppm) (Fig. 11, Table 2).

Cassiterite U-Pb age

Cassiterite grains in the helvine-danalite and its coexisting sphalerite are relatively large (diameter 10–400 μm) and euhedral (Figs. 3f, 4d, 9a). As shown in CL images (Fig. 9b), the cassiterite (in sphalerite) grains show clear alternating bright-dark zoning from core to rim. The cassiterite grains have U contents of 0.20–18.36 ppm (Table 3), and yielded a U-Pb lower-intercept concordia age of 86.5 ± 1.6 Ma (2δ, n = 25, MSWD = 1) (Fig. 10).

DISCUSSION

Formation of oscillatory zoning in helvine-danalite

Oscillatory zoning is common in hydrothermal minerals (e.g. garnet, helvine) (Allegre et al. 1981; Wang and Merino 1992; Jamtveit et al. 1993; Shore and Fowler 1996; Zito and Hanson, 2017; Antao and Salvador. 2019; Raade, 2020). Many previous studies proposed two mechanisms for the formation of oscillatory zoning in hydrothermal minerals: (1) internal crystal growth that involves spontaneous chemical self-organization controlled by kinetic factors, such as the mineral growth rate and the diffusion rate of key mineral-forming elements in the fluid (e.g. Allegre et al. 1981; Wang and Merino 1992); (2) periodic fluctuations of external factors, including pressure-temperature (P-T), fO_2, fS_2, and fluid composition during the crystal growth (e.g. Burt, 1988; Jamtveit et al. 1993; Raade, 2020).

(1) Elemental self-organization helvine-group minerals

At the Dulong, chemical compositions of the helvine-danalite oscillatory zoning vary widely (Figs. 6-7; Table 1). In general, the helvine zones contain much higher Mn, K, Al, Ca, Sc and Y contents but much lower Fe, Zn, Mg, P and Sn content than the danalite zones. The Al, Mg, Mn, Zn and Fe contents vary across different zones, locally up to two orders of magnitude (Fig. 6), and thus achieving that via chemical self-organization is highly unlikely (Kohn, 2004).

(2) Hydrothermal fluid composition

Some authors consider that for the formation of genthelvite-helvine zoning (and other complex zoning), the cation availability (notably Mn, Fe, and Zn) in the fluid is highly important (e.g. Raade 2020). However, our helvine-danalite samples occur mainly in massive sphalerite ores, and the sphalerite shows significant pyrrhotite exsolution (Fig. 3e-f). This implies that neither Zn or Fe was lacking in the helvine-forming fluid. Genthelvite minerals are absent from core to rim in the helvine-danalite, suggesting that fluctuations of the fluid Mn, Fe, and Zn contents were unlikely the main cause for the helvine oscillatory zoning. Meanwhile, published studies on the helvine oscillatory zoning show no fixed growth sequence from core to rim, e.g. Mn → Fe → Zn (e.g. Dunn et al. 1976; Haapala et al. 1972; Langhof et al. 2000; Zito and Hanson 2017), Zn → Fe → Mn (e.g. Clark and Fejer 1976), Fe → Zn (e.g. Kwak and Jackson 1986), or Zn → Mn (e.g. Perez et al. 1990; Raade 2020). This further supports that that elemental composition in the hydrothermal fluid has probably played little role in the formation of oscillatory zoning in helvine-group minerals.

(3) Sulfur fugacity

Considering the decreasing chalcophilicity of Zn ≥ Fe > Mn, sphalerite would form preferentially instead of genthelvite under high-fS_2 conditions, and thus genthelvite is mainly formed in low-fS_2 environment (Burt, 1980). Helvine and danalite are unstable under low-fS_2

conditions, and thus their formation requires relatively high fS_2, under which genthelvite would break down into sphalerite, phenakite, and quartz (Burt 1988). Therefore, the genthelvite formation is highly sensitive to the fluid fS_2. Zinc content (genthelvite mol.%) fluctuations may reflect fS_2 variation: lower Zn content in the helvine zone (cf. danalite zone) reflects higher fS_2, which is also indicated by the high coexisting sulfide (sphalerite) content in the former (Fig. 4b). At Dulong, the presence of coexisting helvine-danalite with sphalerite and the absence of genthelvite thus indicate a high-fS_2 metallogenic environment. From core to rim in the Be mineral samples (Fig. 6a), their Zn contents vary across different zones (Fig. 6c). Overall, three pluses in the Zn content were observed. In the firstly two pluses, the Zn contents increase first and then decrease, indicating that the fS_2 increases first and then drops. In the last pulse, the Zn contents increase continuously, suggesting rising fS_2 in the rim during the Be mineral formation.

(4) Oxygen fugacity

Apart from fS_2, the stability of danalite is also highly sensitive to fO_2, and the mineral is stable only in a very narrow fO_2 range between fayalite (low fO_2) and hematite-magnetite (high fO_2) (Nimis et al. 1996; Burt 1980). SEM imaging indicates the coexistence of cassiterite and ilmenite in the danalite zones (Fig. 4d-f), a phenomenon that is absent in the helvine zone. The presence of these oxides implies that danalite is formed in a higher fO_2 environment. Therefore, during the oscillatory zoning formation from core to rim (Fig.6c), the helvine → danalite transition may signify a fluid fO_2 rise, whilst the formation of internal zones danalite →helvine (Fig.6c) likely suggests a fluid fO_2 drop.

In conclusion, helvine-group minerals are unique in the way that they are not purely sulfides or purely silicates, and thus the coupling of fS_2 and fO_2 influence can reasonably explain the zoning

formation. As mentioned above, we considered that the Dulong helvine zones were formed under higher fS_2 and lower fO_2 conditions than the danalite zones. Periodic and coupled fluctuations of the fluid fS_2 and fO_2 may have formed the distinct oscillatory zoning observed in the helvine-danalite, in agreement with the conclusion by Raade (2020).

Occurrence and substitution mechanism of trace elements in helvine-danalite

The limited available studies suggest that helvine-group minerals are commonly rich in Ca, Al, Sn, Sc, and Y (e.g. Raimbault and Bilal 1993; Zito and Hanson 2017; Raade 2020). LA-ICP-MS data show that the helvine-group minerals from Dulong contain relatively high contents of Mg, Al, P, Ca, Y, Sc, Sn (from several hundred ppm to thousand ppm) and REE (from several ppm to hundreds of ppm), and their concentrations vary distinctly in the helvine zones and danalite zones (Figs. 7 and 8). The molecular formula of Helvine-group minerals can be expressed as $M_4[BeSiO_4]_3S$ and the divalent *M* cation occupies the triangular pyramidic position of the 4-fold coordination, whilst the S atom is positioned in the apex of the pyramid (Hassan and Grundy 1985; Nimis et al. 1996). Compared to the other elements, the difference between the $\sum M$ position element and the theoretical value (4*apfu*) is the largest, with the former far lower than its theoretical value (Table 1). This indicates that the $\sum M$ position would be easily substituted by other trace elements. EPMA results indicate that the elemental variations between the helvine and danalite zones are only shown in the compositional difference at the $\sum M$ position. The Si, **Be, and S compositions are rather fixed, and the differences in elemental features (e.g. ionic radius, chalcophile) at the *M* position may have been the main control for the trace elemental compositions, a viewpoint consistent with many previous studies (Raimbault and Bilal 1993; Zito and Hanson 2017; Raade 2020). The atomic radii and chalcophilicity indices of the major elements and (main) trace elements

309 measured are shown in Figure 11.

310 (1) K, Ca, and P

311 Under 4-fold coordination, the ionic radii of K^+ (1.27 Å) and P^{5+} (0.17 Å) are rather different
312 from those of Mn^{2+} (0.80 Å), Fe^{2+} (0.63 Å) and Zn^{2+} (0.60 Å) in the *M* position (Fig. 11), which
313 makes substitution unlikely from an ionic radius perspective. Although no Ca^{2+} ionic radius data
314 (under 4-fold coordination) were given by Shannon (1976), the Ca^{2+} ionic radius (under 6-fold
315 coordination: 1 Å) is still rather different from that of Mn^{2+}, Fe^{2+} and Zn^{2+} (under 6-fold
316 coordination), which means that Ca^{2+} does not easily enter the helvine crystal lattice. Meanwhile,
317 BSE imaging shows that helvine-danalite contains significant amount K-, Ca- and P-rich minerals,
318 such as biotite, apatite and fluorite (Fig. 4 c, d, f). Therefore, we consider that the K, Ca, and P occur
319 mainly as micro-inclusions in the helvine-danalite matrix.

320 (2) Al and Mg

321 In view of the similar ionic radius among Mg^{2+}, Fe^{2+} and Zn^{2+} under 4-fold coordination
322 (Fig.11) and the good positive Mg vs. (Fe + Zn) correlation (Figs. 6d), we consider Mg substitutes
323 readily Zn and Fe at the *M* position. Under 4-fold coordination, the ionic radius of Al^{3+} is rather
324 different from that of the M-site cations, and its chalcophilicity is also not similar (Fig. 11). EPMA
325 results show that the contents of Al is well correlated to those of Mn (Fig. 6d), suggesting that Al
326 can be incorporated into the helvine-group minerals by substituting Mn. This indicates that trace
327 element distributions in the helvine-group minerals are influenced by the atomic radius, elemental
328 chalcophilicity, and external factors including the fluid fS_2, fO_2, and crystal structure. The trivalent
329 cation (e.g. Al^{3+}) entering the tetrahedron position is required in the coupled substitution to maintain
330 the charge balance of the crystal structure (e.g. Smith et al. 2004; Gaspar et al. 2008). At Dulong,

both the helvine and danalite zones contain relatively high total (∑) REE contents (up to 1500 ppm). Al has good linear relation with *M position* elements and REE indicate that the helvine-group minerals may have coupled substitution mechanism of Al and REEs: $Al^{3+}+REE^{3+}+\square = 3M^{2+}$ (Fig. 12a)

(3) Sn, Sc, and Y

Radde (2020) considered that although Sn^{2+} has higher chalcophilicity than Sn^{4+}, the Sn in helvine-group minerals is more likely to be Sn^{4+} from a stereochemical perspective. Under 4-fold coordination, the ionic radius of Sn^{4+} is similar to that of Zn^{2+} and Fe^{2+}, but different from that of Mn^{2+} (Fig. 11). Therefore, Sn substitutes readily the Zn and Fe at the *M* position ($Sn^{4+}+\square = 2(Fe, Zn)^{2+}$). This is supported by the content of Sn in danalite is much higher than that in helvine(Fig. 7), consistent with the results by Radde (2020). Many studies have reported high Sc contents in helvine-group minerals (Raimbault and Bilal 1993; Zito and Hanson 2017; Raade ,2020). For instance, Radde (2020) reported that the Sc_2O_3 in helvine can reach 1.53 wt.%, and argued that Sc substitutes into the *M* position via $2Sc^{3+}+\square = 3(Mn, Fe, Zn)^{2+}$. The Dulong helvine-danalite samples have also relatively high Sc content (up to 100ppm), with that in the helvine zone higher than that in the danalite zone (Fig. 7). Although no Sc^{3+} ionic radius data (under 4-fold coordination) were given by Shannon (1976), elemental chalcophilicity behavior analysis suggests that Sc is a strongly-lithophile element, and is thus similar to Mn from a chalcophilicity perspective (Christy 2018). This could explain the relatively high Mn content in helvine, although the possible influence from Sc-bearing mineral micro-inclusions in helvine cannot be excluded. Compared with the reported Y contents in helvine-group minerals (Zito and Hanson 2017), the helvine-danalite from Dulong have anomalously high Y contents (up to 1200 ppm), with the helvine zones being especially rich Y (Fig.

353 7). Under 4-fold coordination, Y^{3+} has more similar ionic radius to Mn^{2+} than that of Zn^{2+} and Fe^{2+}.
354 From an ionic radius perspective, therefore, Y can readily substitute Mn in the M-site cations, which
355 is consistent with the high Y content measured in the Dulong helvine.this is Therefore, Y may enter
356 the M-site cations via $2Y^{3+} + \square = 3Mn^{2+}$.

357 In conclusion, the K, P, and Ca occur mainly in helvine-group minerals as micro-inclusions,
358 whilst the Mg, Sn, Y, and Sc can enter readily the M-site cations of helvine-group minerals through
359 isomorphic substitution of Mn, Fe, and Zn. Coupled substitution between Al and REEs into the *M*
360 position may have occurred.

361 **REE in helvine-danalite**

362 Since Y and REE^{3+} have very similar geochemical behavior in hydrothermal minerals (e.g.
363 garnet), if the entry of these elements into garnet is only controlled by the crystal chemical factor
364 (e.g. coupled substitution mechanism), REE^{3+} contents would be strongly related to Y (Dziggel et
365 al. 2009; Park et al. 2017), this phenomenon is also found in our helvine-danalite samples (Fig. 12b).
366 This indicates that the Dulong helvine-danalite has similar coupled substitution behavior for REEs
367 and Y to that in hydrothermal garnet: $REE^{3+} + Y^{3+} \rightarrow 3\ (Mn, Fe, Zn)^{2+}$.

368 HREE-enrichments in helvine were reported in many previous studies (Raimbault and Bilal
369 1993; Zito and Hanson 2017). However, the HREE-enrichment mechanism in helvine remains
370 unclear. For example, Raimbault and Bilal (1993) considered that the HREE-enrichment in helvine
371 may have been crystallographic-control, similar to the REE geochemical behavior in garnet (REEs
372 substitute readily major elements of Fe, Mn, and Zn). Zito and Hanson (2017) considered that the
373 HREE-enrichments in helvine are related to F-rich fluid, as supported by thermodynamic calculation
374 models. Equilibrium constant of the HREE-F complexes is higher than that of the LREE-F

375 complexes, and thus F complexes preferentially with HREEs and forms the HREE enrichments in
376 helvine-group minerals (Gramaccioli et al. 1999; Gramaccioli and Pezzotta 2000). Published REE
377 analyses on helvine-group minerals did not systemically analyze Y or P (Raimbault and Bilal, 1993;
378 Zito and Hanson, 2017), and hence the influence of these element on REE-enrichment is poorly
379 constrained. Our results indicate that the Dulong helvine-danalite contains high contents of HREEs,
380 Y and P, and these elements show good mutual linear relations (Fig. 12b,c). Meanwhile, helvine
381 commonly precipitates under relatively alkaline conditions (Perez et al. 1990; Finch 1990; Burt
382 1977, 1980), and fluorine and phosphate ions can effectively complex with REEs (esp. HREEs)
383 (Mineyev 1963; Sillen and Martell 1964; Dumonceau et al. 1979). We considered that the HREE
384 enrichments in the Dulong helvine-danalite are attributed to the F-Y(-P) enrichments in the ore
385 fluids.

386 It is noteworthy that the Dulong helvine-danalite samples show distinct negative Eu anomalies
387 in chondrite-normalized REE distribution patterns. Previous studies indicate that the Eu decoupling
388 (expressed as positive or negative anomalies) in REEs requires valence changes of Eu, which in
389 turn requires changes in the fluid redox conditions. Fluid redox conditions are commonly co-
390 influenced by the fluid temperature-pressure, fO_2, pH, and chemical compositions (Bau 1991; Wood
391 1990; Slack et al. 2000), and the main control for the type of REE occurrence is temperature
392 (Sverjensky 1984; Bau 1991). Theoretical calculation indicates that when the temperature is >
393 250 °C, Eu occurs mainly as Eu^{2+} (Sverjensky 1984). Published fluid inclusion microthermometric
394 studies on the sulfide-coexisting minerals from Dulong (fluorite, dolomite, quartz, and calcite)
395 yielded ore-formation temperature of 204–398 °C (Ye et al. 2016), under which Eu in the fluid
396 should occur mainly as Eu^{2+}. Therefore, during the helvine-group minerals precipitation at Dulong,

the fluid Eu may have mainly occurred as Eu^{2+}. The reduction of Eu^{3+} to Eu^{2+} is accompanied by increase in ionic radius, and the decrease of adsorption capacity of Eu^{2+} (compared to other REEs) on the helvine-danalite mineral surface, which eventually generates the observed negative Eu anomalies.

Regional Be mineralization potential in the Laojunshan orefield

The Be minerals in the Laojunshan orefield comprise mainly oscillatory-zoned helvine-danalite, with its coexisting cassiterite U-Pb dated to be 86.5 ± 1.6 Ma. The age is consistent (within error) with the reported cassiterite U-Pb ages (87.2 ± 3.9 Ma to 89 ± 1.4 Ma) in the orefield (Wang et al. 2014; Zhao et al. 2018). Published mineralization ages from Dulong (Fig. 13; Liu et al. 2007, 2011; Li et al. 2013; Wang et al. 2014; Xu et al. 2015; Zhao et al. 2018) indicate that both the Be and Sn mineralization are coeval with and likely resulted from the Laojunshan granite intrusion and its associated hydrothermal activities (Liu et al. 2007; Wang et al. 2014; Xu et al. 2015; Zhao et al. 2018). Notably, many Be deposits/prospects have been discovered in the Laojunshan orefield, e.g. the Nanyangtian W deposit and Saxi W-Be (mainly beryl) deposits in the SE Laojunshan orefield, and the Maka W(-Be) (mainly helvine) deposit in the northern Laojunshan orefield. This suggests that the Be mineralization occurred in a regional scale. Recently reported ages for the orefield include high-precision biotite ^{40}Ar-^{39}Ar isochron ages (Nanyangtian: 97.01 ± 1.39 Ma and 99.58 ± 0.98 Ma; Wang et al., 2019), biotite ^{40}Ar-^{39}Ar inverse isochron age (Saxi and Maka: 119 ± 3 Ma; Liu 2011), and zircon U-Pb ages (Maka: 415.6 ± 1.8 Ma, 411.2 ± 3.5 Ma, 400.7 ± 3.0 Ma) of the ore-causative intrusion (Du 2015). These age data imply that the Be mineralization at Dulong, Nanyangtian, and Saxi all occurred in the Cretaceous (Fig. 13), during which the Laojunshan pluton was emplaced. At Maka, the ore-related intrusion is largely coeval (within error) to the Silurian

Nanwenhe granitic gneiss (Liu et al. 2006). As the Nanwenhe granitic gneiss is widespread in the Laojunshan orefield, whether there was an older Early Paleozoic Be mineralization episode in the orefield will need further investigation.

In the southern end of the Laojunshan intrusion (Su et al. 2016), the presence of high-K calc-alkaline and highly-fractionated S-type granite (Liu et al. 2007; Lan et al. 2016; Xu et al. 2015; Zhao et al. 2018) implies that the high Na and K assemblage would preferentially form phenakite and feldspars (instead of beryl), and that the Al would form feldspathoids. This is consistent with previous suggestions that alkali granite-related Be mineralization would form helvine-group minerals instead of beryl (Perez et al. 1990; Finch 1990; Burt 1977, 1980). We therefore suggest that the entire orefield may have substantial Be mineralization potential, which may partly explain why beryl is not found around the Laojunshan intrusion.

IMPLICATIONS

Helvine-group minerals first identified at Dulong Sn-Zn deposits, SE Yunnan. It comprises oscillatory-zoned helvine and danalite, which transition generally (from core to rim) from helvine to danalite but with multiple alternating growth in between. The well-developed oscillatory zoning is likely attributed to the periodic fO_2 and fS_2 fluctuations during the mineral formation, and less related to the fluid compositional variation.

The helvine-danalite from Dulong contains high contents of trace elements (including mainly Ca, Mg, Al, Sc, Sn, Y, and REEs). The Ca, K, and P may have occurred mainly as micro-inclusions in the helvine-danalite, whilst the Sn, Sc, and Y likely enter the helvine (*M* position) via isomorphic substitution. Affected by the ionic radius, elemental chalcophilicity and physicochemical conditions,

441 the Sc and Y preferentially enter helvine, and Sn and Mg into danalite.

442 The helvine-danalite samples are featured by HREE enrichments and negative Eu anomalies,
443 with the ∑REE of helvine distinctly higher than danalite. This may be caused by the higher Y and
444 P in the helvine and higher F in the fluid. F-Y-rich fluid and phosphate ion would preferentially
445 complex HREEs and enter helvine. REE minerals mainly enter helvine through $Y^{3+}+REE^{3+} + \square =$
446 $3(Mn, Fe, Zn)^{2+}$, as well as through coupled substitution of Al with REEs. The dominance of Eu^{2+}
447 for Eu in the fluid may have generated the observed negative Eu anomalies.

448 The helvine-coexisting cassiterite from Dulong is U-Pb dated to be 86.5 ± 1.6 Ma, coeval with
449 the Dulong Sn-Zn polymetallic mineralization. This implies that both are product of the Cretaceous
450 Laojunshan magmatic-hydrothermal activity. Regional mineralization age compilation indicates
451 that Cretaceous (plus possibly Early Paleozoic) Be mineralization is common in the orefield, and
452 the whole orefield has likely substantial potential for Be discovery.

453 **ACKNOWLEDGEMENTS AND FUNDING**

454 We thank the Editor Hongwu Xu, Associate Editor Matthew Steele-Maclnnis and two
455 anonymous reviewers for their comments on our manuscript, and appreciate the assistance of
456 Yunfeng Liu, Suoqing Zhang, and Qinfu Ye from the Yunan Hualian Zinc and Indium Stock., LTD
457 in South Yunnan province and Hang Su from Yunnan Hualian Mineral Exploration Co. LTD during
458 our fieldwork. We would like to acknowledge Yanwen Tang and Junjie Han from the State Key
459 Laboratory of Ore Deposit Geochemistry (SKLODG), Institute of Geochemistry, Chinese Academy
460 of Sciences (IGCAS) for their assistance the experiment. This study was funded by the National
461 Key R & D Program of China (2016YFC0600503).

462

463 REFERENCES

464

465 Allegre, C.J., Provost, A., and Jaupart, C. (1981) Oscillatory zoning: a pathological case of crystal
466 growth. Nature, 294, 223–228.

467 Antao, S.M., and Salvador, J.J. (2019) Crystal Chemistry of Birefringent Uvarovite Solid
468 Solutions. Minerals, https://doi.org/10.3390/min9070395.

469 Bau, M. (1991) Rare-earth element mobility during hydrothermal and metamorphic fluid –rock
470 interaction and the significance of the oxidation state of europium. Chemical Geology, 93, 219–
471 230.

472 Burt, D.M. (1977) Chalcophile-lithophile tendencies in the helvite group: genthelvite stability in the
473 system ZnO–BeO–Al_2O_3–SiO_2–SO–1–F_2O–1 (abstract). American Geophysical Union
474 Transactions 58, 1242.

475 Burt, D.M. (1980) The Stability of danalite, $Fe_4Be_3(SiO_4)_3S$. American Mineralogist, 65, 355–360.

476 Burt, D.M. (1988) Stability of genthelvite, $Zn_4(BeSiO_4)_3S$: An exercise in chalcophilicity using
477 exchange operators. American Mineralogist, 73, 1384–1394.

478 Christy, A.G. (2018) Quantifying lithophilicity, chalcophilicity and siderophilicity. European
479 Journal of Mineralogy 30, 193–204.

480 Clark, A.M. and Fejer, E.E. (1976) Zoned genthelvite from the Cairngorm Mountains, Scotland.
481 Mineralogical Magazine, 40, 637–639.

482 Deer, W.A., Howie, R.A., Wise, W.S., and Zussman, J. (2004) Rock-forming minerals, Vol. 4B:
483 Framework silicates. Second Edition, The Geological Society of London, England, 352–368.

Du, S.J., Wen, H.J., Qing, C.J., Yan, Y.F., Yang, G.S., and Feng, P.Y. (2014) Occurrence of Beryllium in the Maka Tungsten Polymetallic Deposit in Malipo County, Yunnan Province and its Significance. Acta Mineralogica Sinica, 34, 446-450 (in Chinese with English abstract).

Dumonceau, J., Bigot, S., Treuil, M., Faucherre, M., and Fromage, F. (1979) Détermination des constantes de formation des tétracarbonatolanthanidates (III). Rev. Chimie Minerale, 16, 583-592.

Dunn, P.J. (1976) Genthelvite and the helvine-group. Mineralogical Magazine, 40, 627–636

Dziggel, A., Wulff, K., Kolb, J., Meyer, F.M., and Lahaye, Y. (2009) Significance of oscillatory and bell-shaped growth zoning in hydrothermal garnet: evidence from the Navachab gold deposit. Namibia. Chem. Geol. 262, 262–276.

Finch, A.A. (1990) Genthelvite and willemite, zinc minerals associated with alkaline magmatism from the Motzfeldt center, South Greenland. Mineralogical Magazine, 34, 407–412.

Gaspar, M., Knaack, C., Meinert, L.D., and Moretti, R.(2008) REE in skarn systems: a LA-ICP-MS study of garnets from the Crown Jewel Deposit. Geochimica et Cosmochimica Acta, 72, 185–205.

Gramaccioli, C.M., and Pezzotta, F. (2000) Geochemistry of yttrium with respect to the rare-earth elements in pegmatites. Memorie della Italiana di Scienze e del Museo Civico di Storia Naturale di Milano XXX, 111–115.

Gramaccioli, C.M., Diella, V., and Demartin, F. (1999) The role of fluoride complexes in REE geochemistry and theimportance of 4f electrons: some examples in minerals. European Journal of Mineralogy, 11, 983–992.

Goldschmidt, V.M (1932) Geochemische Leit-Elemente. Naturwissenschaften, 20, 947-948.

Grew, E. S., and Hazen, R. M. (2014) Beryllium mineral evolution. American Mineralogist, 99(5-6), 999-1021.

Haapala, I. and Ojanpera, P. (1972) Genthelvite-bearing greisens in southern Finland. Bulletin of the Geological Survey of Finland, 259, 22.

Hassan, I., and Grundy, H.D. (1985) The crystal structures of helvite group minerals, (Mn, Fe, Zn)$_8$($Be_6Si_6O_{24}$) S_2. American Mineralogist, 70, 186–192

He, F., Zhang, Q., Liu, Y.P., Ye, L., Miao, Y.L., Wang, D.P., Su, H., Bao, T., and Wang, X.J. (2015) Lead Isotope Compositions of Dulong Sn-Zn Polymetallic Deposit, Yunnan, China: Constraints on Ore-forming Metal Sources. Acta Mineralogica Sinica, 35(3), 32-40 (in Chinese with English abstract).

He, F., Zhang, Q., Wang, D.P., Liu, Y.P., Ye, L., and Bao, T. (2014) Ore-Forming Materials Sources of the Dulong Sn-Zn polymetallic Deposit, Yunnan, Evidences from S-C-O stable isotope. Bulletin of Mineralogy, Petrology and Geochemistry, 33(6), 900-907 (in Chinese with English abstract).

Holten, T., Jamtveit, B., and Meakin, P. (2000) Noise and oscillatory zoning of minerals. Geochimica et Cosmochimica Acta, 11, 1893−1904.

Jamtveit, B., Wogelius, R.A., and Fraser, D.G. (1993) Zonation patterns of skarn garnets: Records of hydrothermal system evolution. Geology, 21, 113–116.

Kohn, M.J., 2004. Oscillatory- and sector-zoned garnets record cyclic (?) rapid thrusting in central Nepal. Geochemistry Geophysics Geosystems, 5, 12.Kwak, T.A.P., and Jackson, P.G. (1986) The compositional variation and genesis of danalite in Sn–F–W skarns, NW Tasmania, Australia. Neues Jahrbuch für Mineralogie - Monatshefte, 452–462.

528 Lan, J.B., Liu, Y.P., Ye, L., Zhang, Q., Wang, D.P., and Su, H. (2016) Geochemistry and age
529 spectrum of Late Yanshanian granites from Laojunshan Area, Southeastern Yunnan Province,
530 China. Acta Mineralogica Sinica, 36(4), 441-454 (in Chinese with English abstract).
531 Langhof, J., Holtstam, D., and Gustafsson, L. (2000) Chiavennite and zoned genthelvite–helvite as
532 late-stage minerals of the Proterozoic LCT pegmatites at Uto, Stockholm, Sweden. GFF, 122,
533 207–212
534 Li, J.K., Wang, D.H., Li, H.Q., Cheng, Z.H., and Mei, Y.P. (2013) Late Jurassic-early Cretaceous
535 mineralization in the Laojunshan ore concentration area, Yunnan province. Earth Science-
536 Journal of China University of Geosciences, 38(5), 1023-1036 (in Chinese with English
537 abstract).
538 Li, J.K., Zou, T.R., Wang, D.H., and Ding, X. (2017) A review of beryllium metallogenic regularity
539 in China. Mineral Deposits, 36(4), 951-978 (in Chinese with English abstract).
540 Liu, Y.S., Hu, Z.C., Gao, S., Günther, D., Xu, J., Gao, C.G., Chen, H.H. (2008) In situ analysis of
541 major and trace elements of anhydrous minerals by LA-ICP-MS without applying an internal
542 standard. Chemical Geology, 257, 34-43.
543 Liu, Y.P., Li, Z., Li, H., Guo, L., Xu, W., Ye, F., Li, C., Pi, D. (2007) U–Pb geochronology of
544 cassiterite and zircon from the Dulong deposit: evidence for Cretaceous large-scale granitic
545 magmatism and mineralization events in southeastern Yunnan Province, China. Acta Petrol Sin,
546 23, 967–976 (in Chinese with English abstract).
547 Liu, Y.P., Ye, L., Li, C.Y., Song, B., Li, T.S., Guo, L.G., and Pi, D.H. (2006) Discovery of the
548 Neoproterozoic magmatics in southeastern Yunnan: evidence from SHRIMP zircon U-Pb
549 dating and lithogeochemistry. Acta Petrol Sin, 22, 916–926 (in Chinese with English abstract).

550 Liu, Y.S., Hu, Z.C., Zong, K.Q., Gao, C.C., and Chen, H.H. (2010) Reappraisement and refinement
551 of zircon U-Pb isotope and trace element analyses by LA-ICP-MS. Chinese Science Bulletin,
552 55(15), 1535-1546
553 Liu, Y.P., Li, Z.X., Ye, L., Tan, H.Q., and Li, C.Y. (2011) Ar-Ar chronology of Tungsten
554 mineralization in Laojunshan ore concentration area. Acta Mineralogica Sinica, (S1), 617-618 (in
555 Chinese).
556 Mineyev, D.A. (1963) Geochemical differentiation of the rare earths. Geochemistry, 1129-1149
557 Nimis, P., Molin, G., and Visona, D. (1996) Crystal chemistry of danalite from Daba Shabeli
558 Complex (N Somalia). Mineralogical Magazine, 60, 375–379.
559 Park, C., Song, Y., Kang, I.M., Shim, J., Chung, D., and Park, C.S. (2017) Metasomatic changes
560 during periodic fluid flux recorded in grandite garnet from the Weondong W skarn deposit,
561 South Korea. Chemical Geology, 451, 135–153.
562 Perez, J.B., Dusausoy, Y., Babkine, J., and Pagel, M. (1990) Mn zonation and fluid inclusions in
563 genthelvite from the Taghouaji complex (Air Mountains, Niger). American Mineralogist, 75,
564 909–914.
565 Raade, G. (2020) Helvine-group minerals from Norwegian granitic pegmatites and some other
566 granitic rocks: cases of significant Sc and Sn contents. Canadian Mineralogist, 58(3), 367-379
567 Ragu, A. (1994) Helvite from the French Pyrénée as evidence for granite-related hydrothermal
568 activity. Canadian Mineralogist, 32, 111–120.
569 Raimbault, L., and Bilal, E. (1993) Trace-element contents of helvite-group minerals from
570 metasomatic albitites and hydrothermal veins at Sucuri, Brazil, and Dajishan, China. Canadian
571 Mineralogist, 31, 119–127.

572 Shannon, R.D. (1976) Revised effective ionic radii and systematic studies of interatomic distances
573 in halides and chalcogenides. Acta Crystallographica, A32, 751–767.
574 Shore, M., and Fowler, A.D. (1996) Oscillatory zoning in minerals: A common phenomenon.
575 Canadian Mineralogist, 34, 1111–1126.
576 Sillen, L.G., and Martell, A.E. (1964) Stability constraints of metal-ion complexes. Chem. Soc.
577 London, Spec. Publ. 17.
578 Slack, J.F., Meier, A.L., Malcolm, M.J., Fey, D.L., Doughten, M.W., and Wanless, G.A.(2000)
579 Trace element and rare-earth element geochemistry of bedded and massive sulfides from the
580 Sullivan Pb–Zn–Ag deposit, British Columbia—a reconnaissance study. In: Lydon, J.W., Hoy,
581 T., Slack, J.F., Knapp, M.E. (Eds.), The Geological Environment of the Sullivan Pb –Zn –Ag
582 Deposit, British Columbia. Spec. Publ.-Geol. Assoc. Can. Miner. Depos. Div., vol. 1, pp. 720–
583 735.
584 Smith, M.P., Henderson, P., Jeffries, T.E.R., Long, J., and Williams, C.T. (2004) The rare earth
585 elements and uranium in garnet from the Beinn an Dubhaich aureole, Skye, Scotland, UK:
586 constraints on processes in a dynamic hydrothermal system. Journal of Petrology, 45, 457–484.
587 Su, H., Wei, W.B., Tao, Z.H., Dao, X.Q., and Li, T.J. (2016) Geological and Geochemical
588 Characteristics of Later Yanshanian Concealed Granite and its Relation with Sn-Zn
589 Polymetallic Mineralization. Acta Mineralogica Sinica, 36(4), 488-496 (in Chinese with
590 English abstract).
591 Sverjensky, D.A. (1984) Europium redox equilibria in aqueous solution. Earth and Planetary
592 Science Letters, 67, 70–78.

593 Taylor, S.R., and McLennan, S.M. (1995) The geochemical evolution of the continental
594 crust. Reviews of Geophysics, 33(2), 241-265.
595 Wang, C.Y., Han, R.S., Huang, J.G., Xu, S.H., and Ren, T. (2019). The ^{40}Ar–^{39}Ar dating of biotite
596 in ore veins and zircon U–Pb dating of porphyritic granite dyke in the Nanyangtian tungsten
597 deposit in SE Yunnan, china. Ore Geology Reviews, https://doi.org/10.1016/j.ore_geo
598 rev.2019.103133.
599 Wang, X.J., Liu, Y.P., Miao, Y.L., Bao, T., Ye, L., and Zhang, Q. (2014). In LA-MC-ICP-MS
600 cassiterite U-Pb dating of Dulong Sn-Zn polymetallic deposit and its significance. Acta
601 Petrologica Sinica, 30, 867-876 (in Chinese with English abstract).
602 Wang, Y.F., and Merino, E. (1992) Dynamic model of oscillatory zoning of trace elements in calcite:
603 Double layer, inhibition, and self-organization. Geochimica et Cosmochimica Acta, 56, 587–
604 596.
605 Wood, S.A. (1990) The aqueous geochemistry of the rare-earth elements and yttrium: 2. Theoretical
606 predictions of speciation in hydrothermal solutions to 350 °C at saturation water vapor pressure.
607 Chemical Geology, 88, 99–125.
608 Xu, B., Jiang, S.Y., Wang, R., Ma, L., Zhao, K.D., and Yan, X. (2015) Late Cretaceous granites from
609 the giant Dulong Sn-polymetallic ore district in Yunnan Province, South China: geochronology,
610 geochemistry, mineral chemistry and Nd–Hf isotopic compositions. Lithos, 218: 54–72.
611 Yan, D.P., Zhou, M.F., Wang, C.Y., and Xia, B. (2006) Structural and geochronological constraints
612 on the tectonic evolution of the Dulong-Song Chay tectonic dome in Yunnan province, SW
613 China. Journal of Asian Earth Sciences, 28, 332–353.

614 Ye, L., Bao, T., Liu, Y.P., He, F., Wang, X.J., Zhang, Q., Wang, D.P., and Lan, J.B. (2018) The trace
615 and rare elements in scheelites and their implication for mineralization in Dulong Sn-Zn
616 polymetal ore deposit, Yunnan Province. Journal of Nanjing University (Natural Science),
617 54(2), 245-258 (in Chinese with English abstract).
618 Ye, L., Bao, T., Liu, Y.P., Zhang, Q., Wang, X.J., He, F., Wang, D.P., and Lan, J.B. (2016)
619 Mineralization Stages and Ore-Forming Fluid of Dulong Sn-Zn Polymetal Ore Deposit,
620 Yunnan Province, China. Acta Mineralogica Sinica, 36(4), 503-509 (in Chinese with English
621 abstract).
622 Ye, L., Liu, Y.P., Zhang, Q., Bao, T., He, F., Wang, X.J., Wang, D.P., and Lan, J.B. (2017) Trace and
623 rare elements characteristics of sphalerite in Dulong super large Sn-Zn polymetallic ore deposit,
624 Yunnan province. Journal of Jilin University (Earth Science Edition), 47(3), 734-750. (in
625 Chinese with English abstract).
626 Zhang, R., Lehmann, B., Seltmann, R., Li, C., and Sun, W. (2017) Cassiterite U-Pb geochronology
627 constrains magmatic-hydrothermal evolution in complex evolved granite systems: The classic
628 Erzgebirge tin province (Saxony and Bohemia). Geology, 45, 1095–1098.
629 Zhang, W.L., Che, X.D., Wang, R.C., Xie, L., Li, X.F., Zhang, D. (2020) Optimum conditions for
630 quantitative analysis of beryllium by electron probe microanalysis: a case study of beryl.
631 Chinese Science Bulletin, dol: 10.1360/TB-2020-0316
632 Zhao Z, Hou L, Ding J, Zhang Q, Wu S (2018) A genetic link between Late Cretaceous granitic
633 magmatism and Sn mineralization in the southwestern South China Block: a case study of the
634 Dulong Sn dominant polymetallic deposit. Ore Geology Reviews , 93, 268–289

635 Zito, G., and Hanson, S.L. (2017) Genthelvite overgrowths on danalite cores from a Pegmatite
636 Miarolitic Cavity in Cheyenne Canyon, El Paso County, Colorado. Canadian Mineralogist, 55,
637 195-206

638

639 **Figure Captions**

640 **Figure 1 a** Simplified structural map showing the location of the study area. **b** Geological sketch
641 map of the Laojunshan Metamorphic Core Complex in SE Yunnan, SW China (modified after Liu
642 et al. 2006). **c** Geological map of the Dulong Sn-polymetallic skarn deposit (modified after Liu et
643 al. 2007)

644

645 **Figure 2** XRD (a) and Raman (b) images of helvine-group minerals from the Dulong Sn-Zn
646 polymetallic deposit. Abbreviations: Dan = danalite; Sp = sphalerite; Po = pyrrhotite; Bt = biotite;
647 DL= samples from Dulong district; RRUFF mineral = RRUFF Raman database (http://rruff.info)

648

649 **Figure 3** Hand specimen photographs **(a-b);** thin-section microphotographs under crossed-
650 polarized light **(c-d)** and reflected light **(e-f),** showing the intergrowth of sphalerite, Biotite,
651 pyrrhotite, cassiterite, talc and helvine-group minerals. Definitions of mineral abbreviations: Dan =
652 danalite; Hel = helvine; Sp = sphalerite; Po = pyrrhotite; Bt = biotite; Tlc = talc. Cst = cassiterite

653

654 **Figure 4** Backscattered electron (BSE) images of helvine-group minerals from Dulong: (**a-b**)
655 euhedral-subhedral oscillatory-zoned helvine-danalite grain, showing intergrowth of sphalerite, talc,
656 biotite and helvine-danalite. In general, the dark-gray and bright zones are helvine and danalite,

657 respectively; **(c)** fluorite veins or grains intergrown with sphalerite and pyrrhotite in the helvine-
658 danalite; (**d-f**) cassiterite, biotite, ilmenite, apatite in the danalite zone. Abbreviations: Ilm = ilmenite;
659 Ap = apatite, and as in Figure 3.
660
661 **Figure 5** Coupled BSE images with EPMA multi-element maps of the helvine-danalite samples: (**a**)
662 BSE image; (**b-h**) EPMA maps of Mn, Fe, Zn, Si, S, Al, and Mg.
663
664 **Figure 6 (a)** BSE image of helvine-danalite grain, showing seven (core-f) zones in the grain; **(b)**
665 chemical compositions of the seven zones; **(c)** EPMA line scan of Fe, Mn, Zn, S, and Si for profiles
666 A-B and C-D in (a); **(d)** a-Correlation diagram of MnO vs. Al_2O_3, b-(ZnO、FeO) vs. MgO
667
668 **Figure 7** Trace element compositions of helvine-group minerals from Dulong
669
670 **Figure 8** Chondrite-normalized REE diagram for the Dulong helvine-group minerals. Chondrite
671 normalizing values are from Taylor and McLennan (1995).
672
673 **Figure 9** Representative cathodoluminescence (CL) images of the cassiterite intergrown with
674 sphalerite and helvine-group minerals
675
676 **Figure 10** Tera-Wasserburg U–Pb age diagrams for the cassiterite from Dulong
677
678 **Figure 11** Plot of ionic charge vs. ionic radius (fourfold coordination except Ca^{2+} and Sc^{3+}; from

679 Shannon 1976) and chalcophilicity index (Christy 2018) for the elements measured

680

681 **Figure 12** Trace element and REE diagrams of helvine-group in Dulong ore district

682

683 **Figure 13** Age range of representative granites and associate Be deposits in the Laojunshan orefield

684 (modified after Liu et al., 2007; Liu et al., 2011; Li et al., 2013; Wang et al., 2014; Du et al., 2015;

685 Xu et al., 2015; Zhao et al., 2018; Wang et al., 2019)

686

687 **Table Captions**

688 Table 1. Major element compositions of the helvine-danalite samples

689 n = number of spots; **BeO calculation with the assumption of Si = 3 and Be = 3.

690 Table 2. Trace element compositions of the helvine-danalite samples

691 Table 3. LA-ICP-MS U–Pb dating results of cassiterite from Dulong ore district

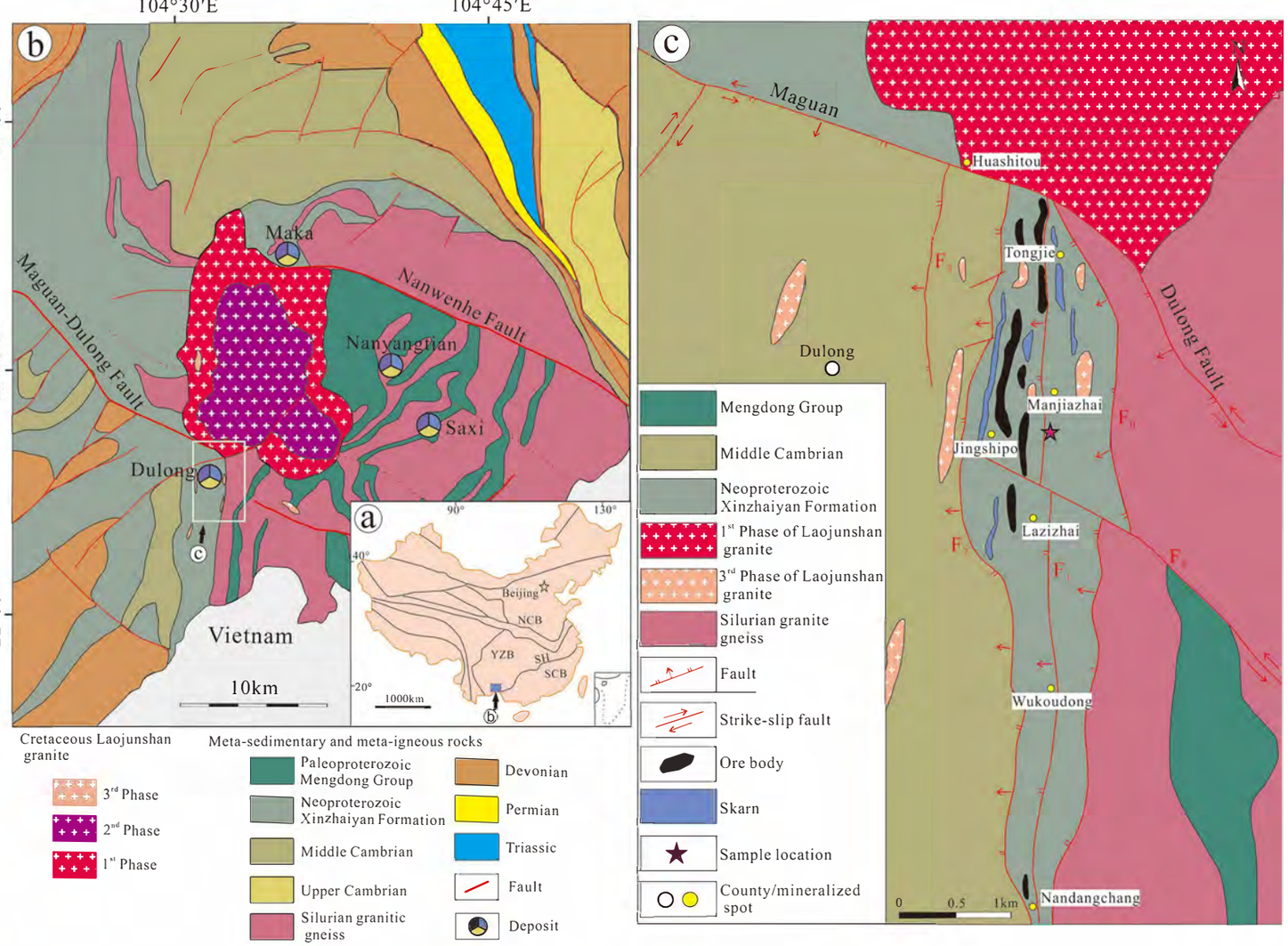
104°30'E
104°45'E
25°00'N
22°30'N
22°00'N
b
Maka
Nanwenhe Fault
Maguan-Dulong Fault
Nanyangjian
Saxi
Dulong
c
Vietnam
10km
a
90°
130°
40°
20°
Beijing
NCB
YZB
SB
SCB
1000km
b
Cretaceous Laojunshan granite
3rd Phase
2nd Phase
1st Phase
Meta-sedimentary and meta-igneous rocks
Paleoproterozoic Mengdong Group
Neoproterozoic Xinzhaiyan Formation
Middle Cambrian
Upper Cambrian
Silurian granitic gneiss
Devonian
Permian
Triassic
Fault
Deposit
c
Maguan
Huashitou
Tongjie
Dulong
Dulong Fault
Manjiazhai
Jingshipo
Lazizhai
Wukoudong
Nandangchang
0
0.5
1km
Mengdong Group
Middle Cambrian
Neoproterozoic Xinzhaiyan Formation
1st Phase of Laojunshan granite
3rd Phase of Laojunshan granite
Silurian granite gneiss
Fault
Strike-slip fault
Ore body
Skarn
Sample location
County/mineralized spot

Fig 1

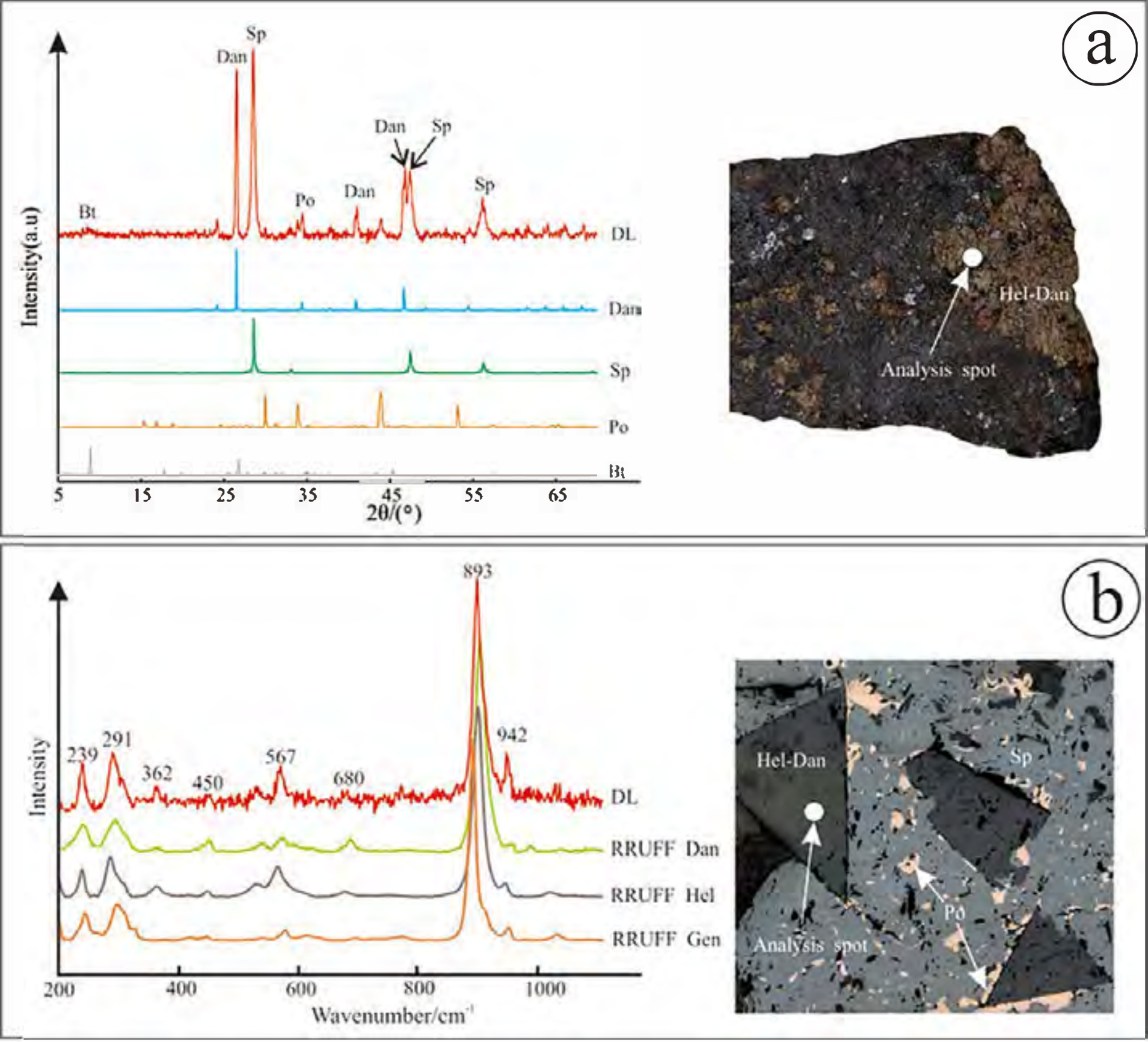
a
Sp
Dan
Dan
Sp
Po
Dan
Sp
Bt
DL
Dan
Sp
Po
Bt
Intensity(a.u)
5
15
25
35
45
55
65
2θ/(°)
Hel-Dan
Analysis spot
b
893
942
291
239
362
450
567
680
DL
RRUFF Dan
RRUFF Hel
RRUFF Gen
Intensity
200
400
600
800
1000
Wavenumber/cm-1
Hel-Dan
Sp
Po
Analysis spot

Fig 2

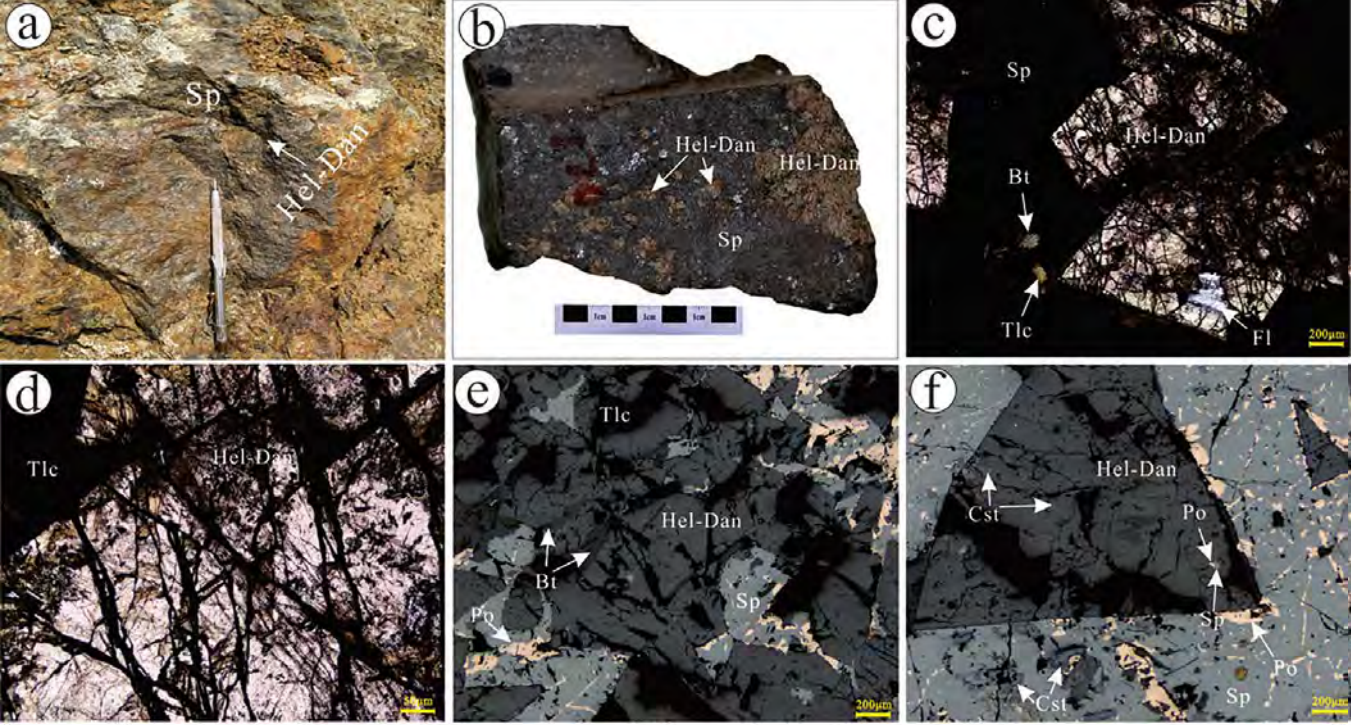
a
Sp
Hel-Dan
b
Hel-Dan
Hel-Dan
Sp
c
Sp
Hel-Dan
Bt
Tlc
Fl
200μm
d
Tlc
Hel-Dan
e
Tlc
Hel-Dan
Bt
Po
Sp
200μm
f
Hel-Dan
Cst
Po
Sp
Po
Cst
Sp
200μm

Fig 3

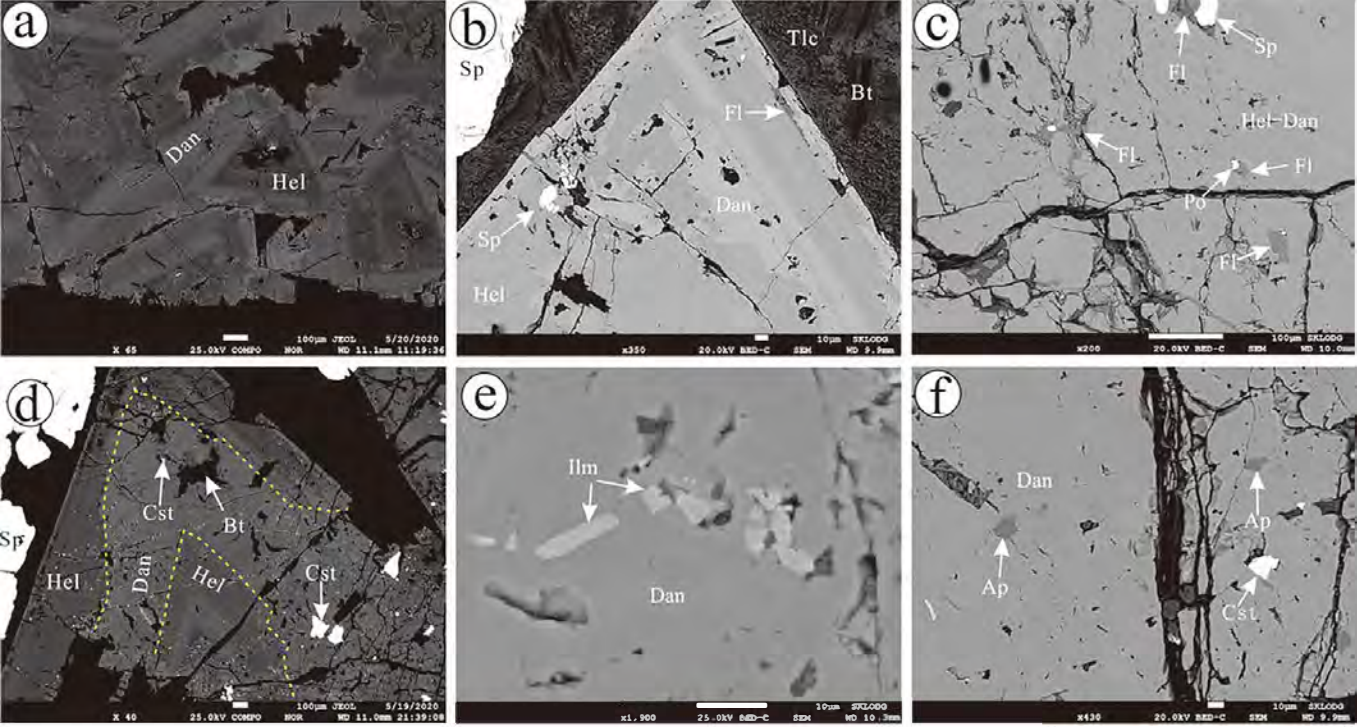
a
Dan
Hel
b
Tlc
Sp
Bt
Fl
Dan
Sp
Hel
c
Sp
Fl
Hel-Dan
Fl
Fl
Po
Fl
d
Cst
Bt
Sp
Hel
Dan
Hel
Cst
e
Ilm
Dan
f
Dan
Ap
Ap
Cst

Fig 4

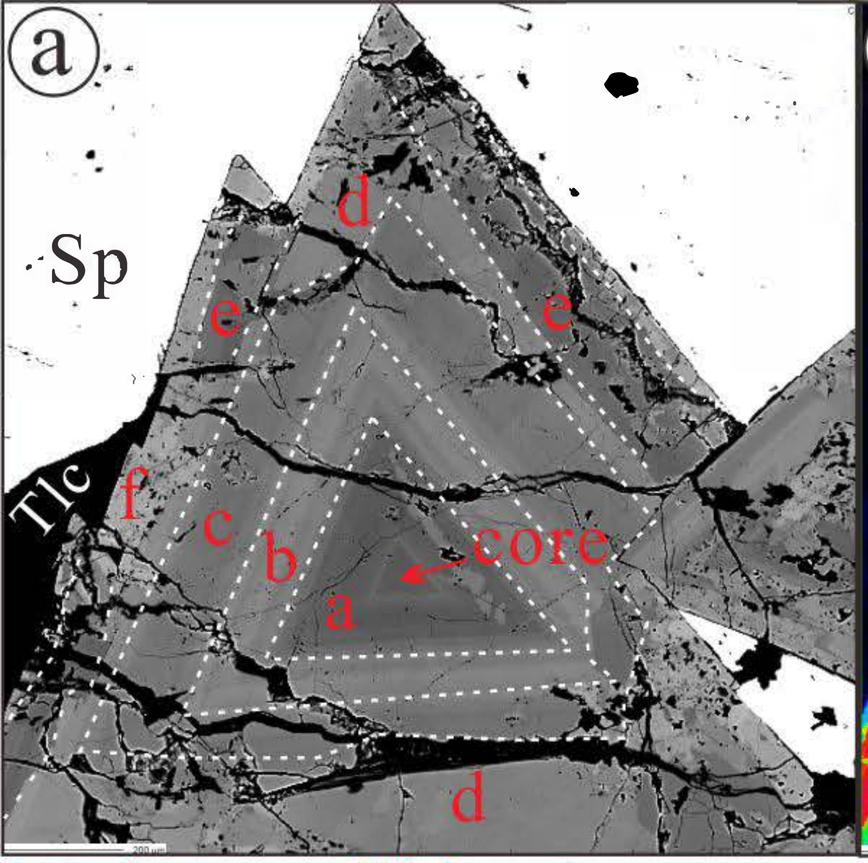

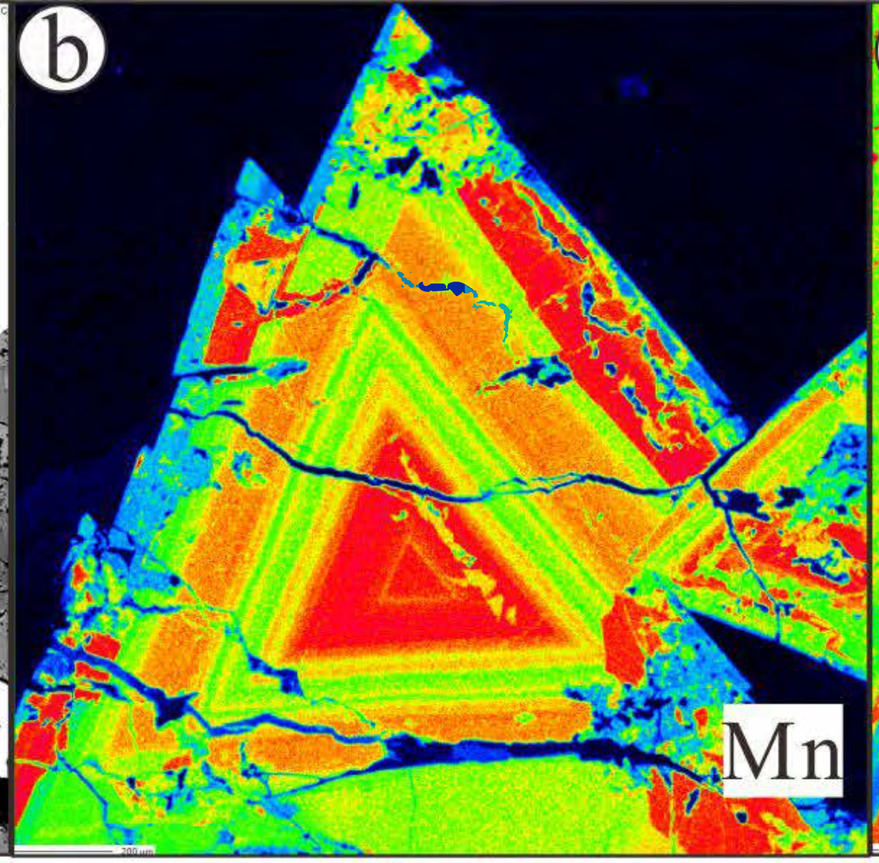

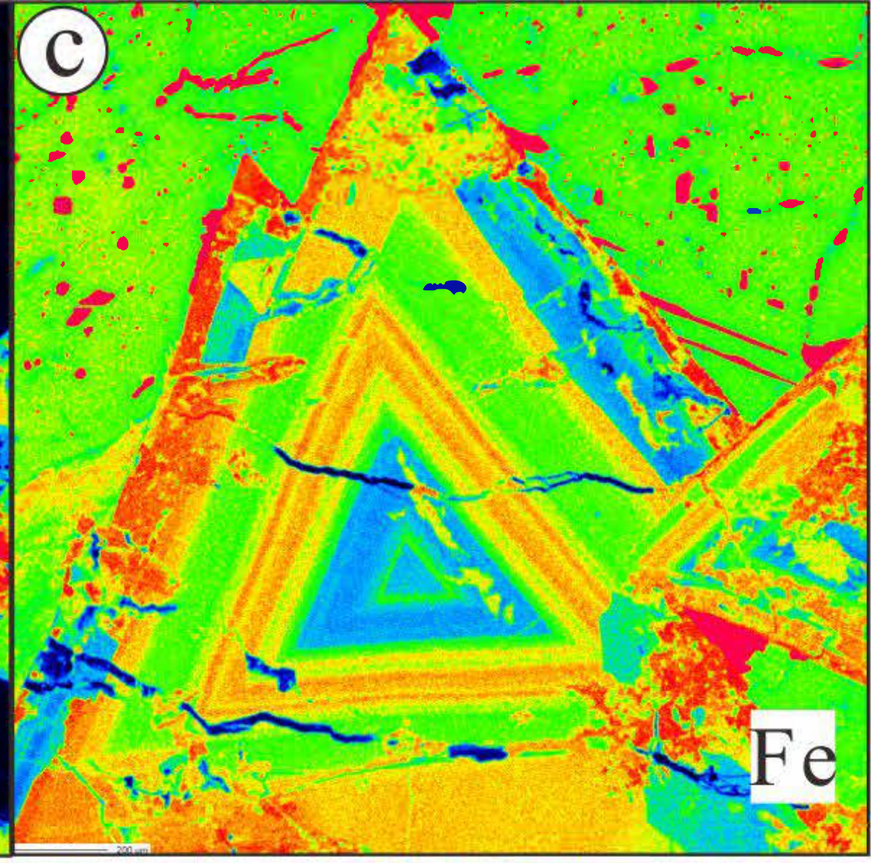

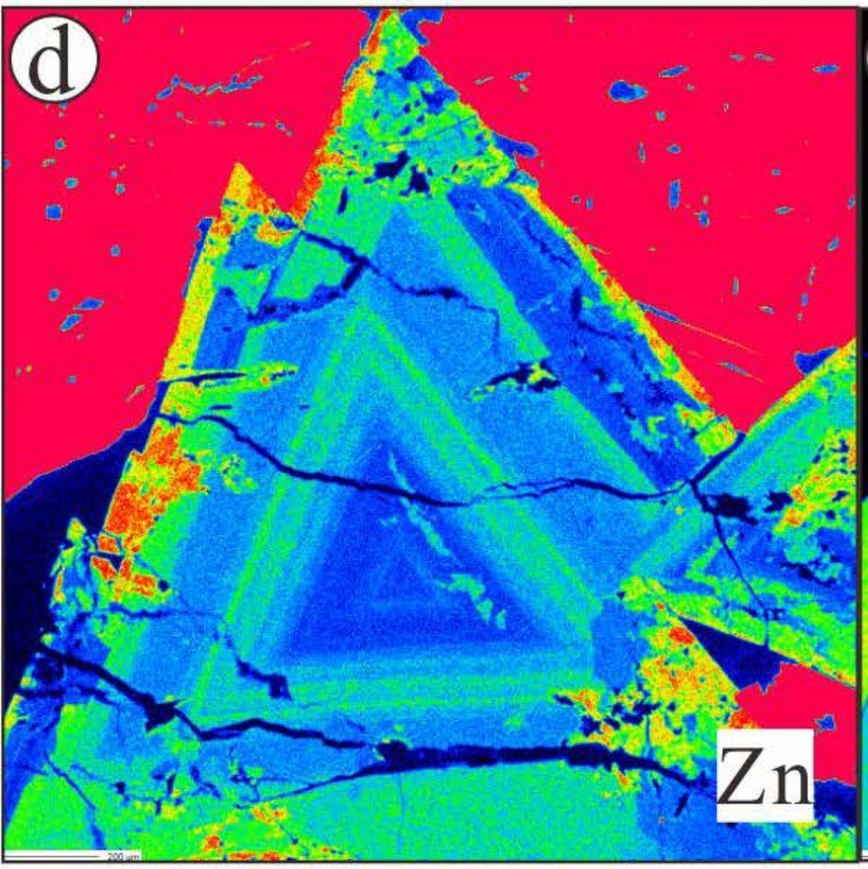

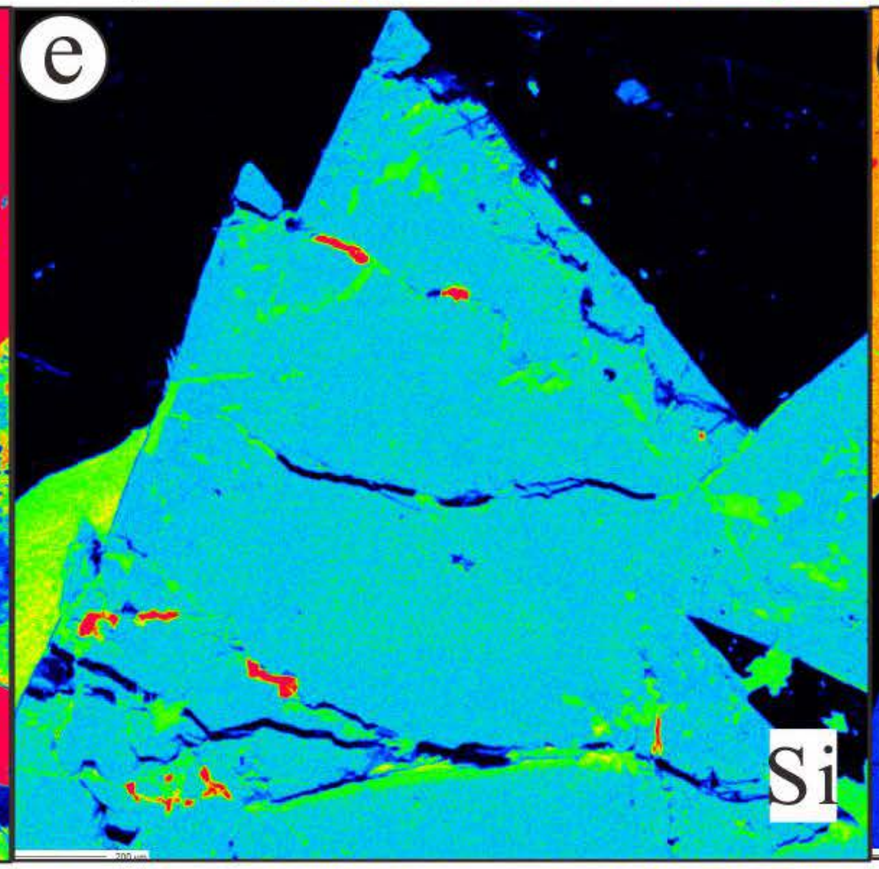

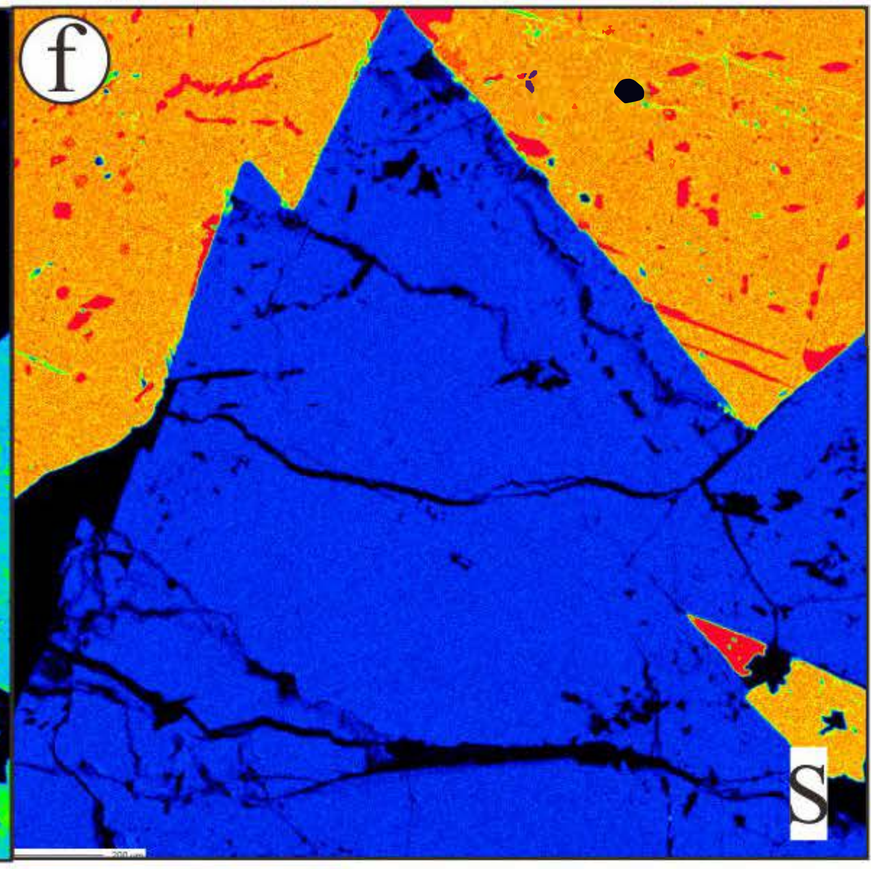

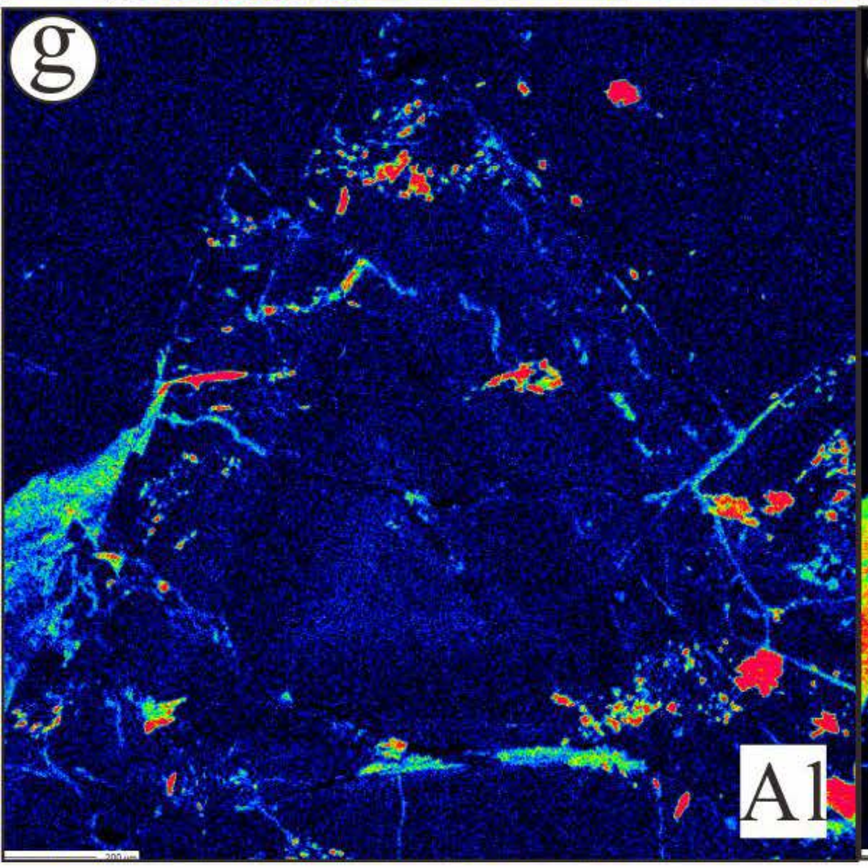

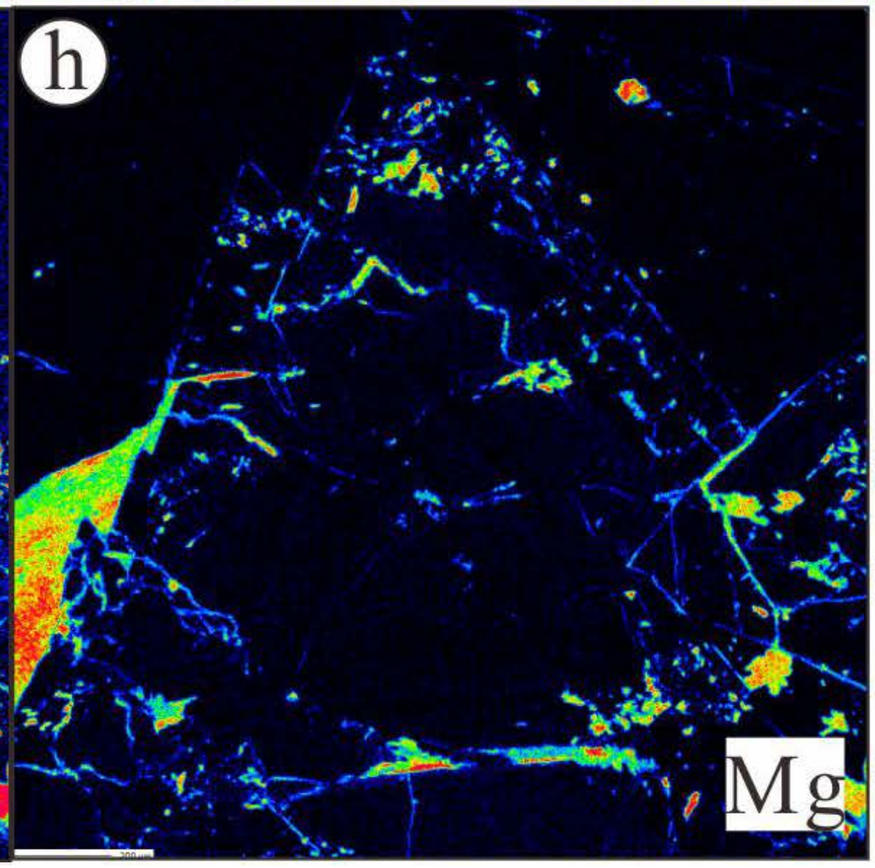

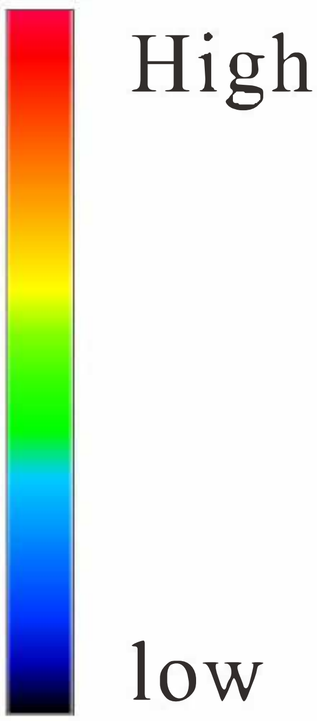

Fig 5

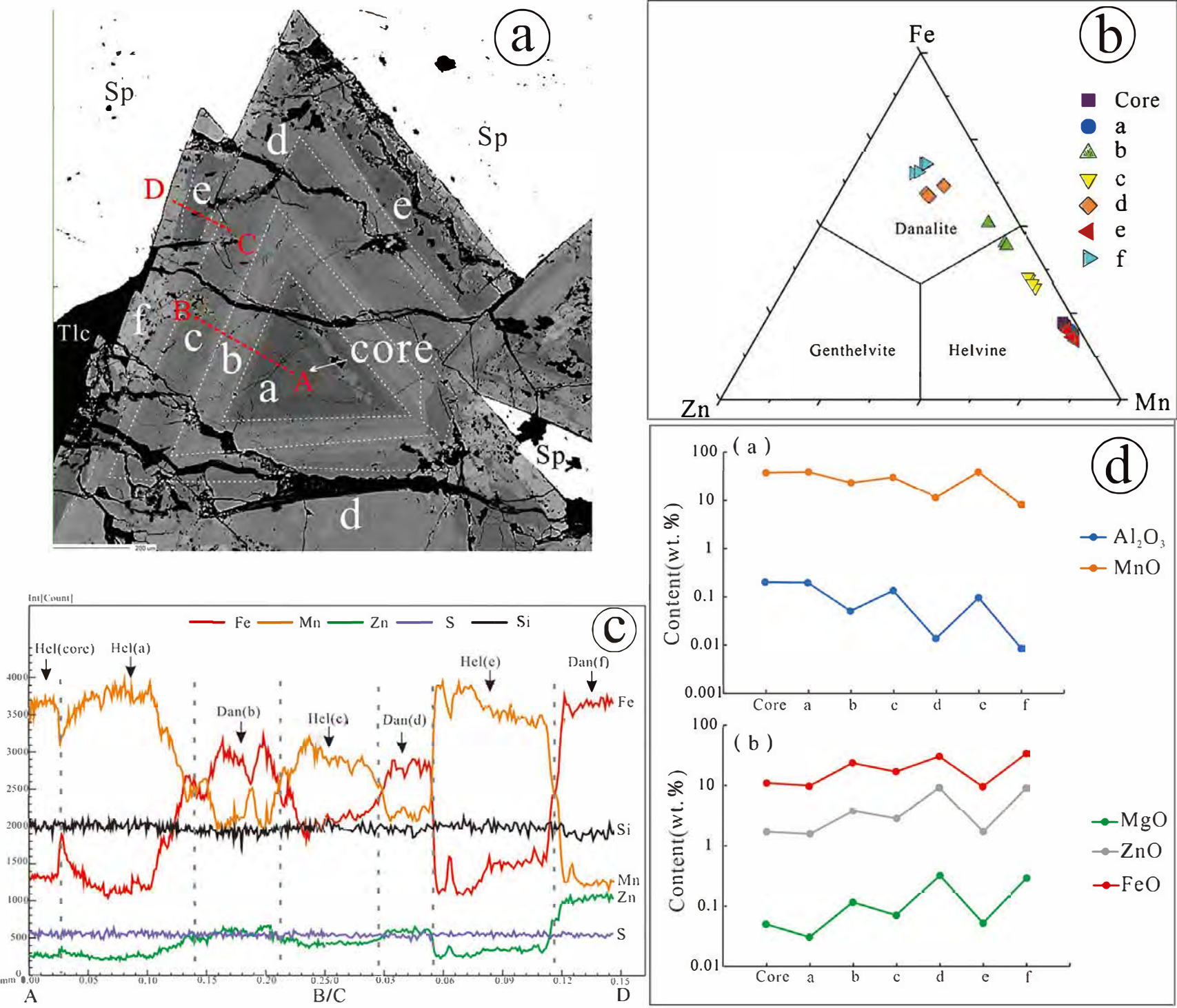
a
Sp
Sp
Sp
Tlc
d
e
e
D
C
f
B
c
b
core
a
A
d
b
Fe
Mn
Zn
Core
a
b
c
d
e
f
Danalite
Genthelvite
Helvine
Zn
Mn
c
Int[Count]
Fe
Mn
Zn
S
Si
Hel(core)
Hel(a)
Dan(b)
Hel(c)
Dan(d)
Hel(e)
Dan(f)
Fe
Si
Mn
Zn
S
A
B/C
D
d
(a)
(b)
Content(wt. %)
Al2O3
MnO
MgO
ZnO
FeO
Core
a
b
c
d
e
f

Fig 6

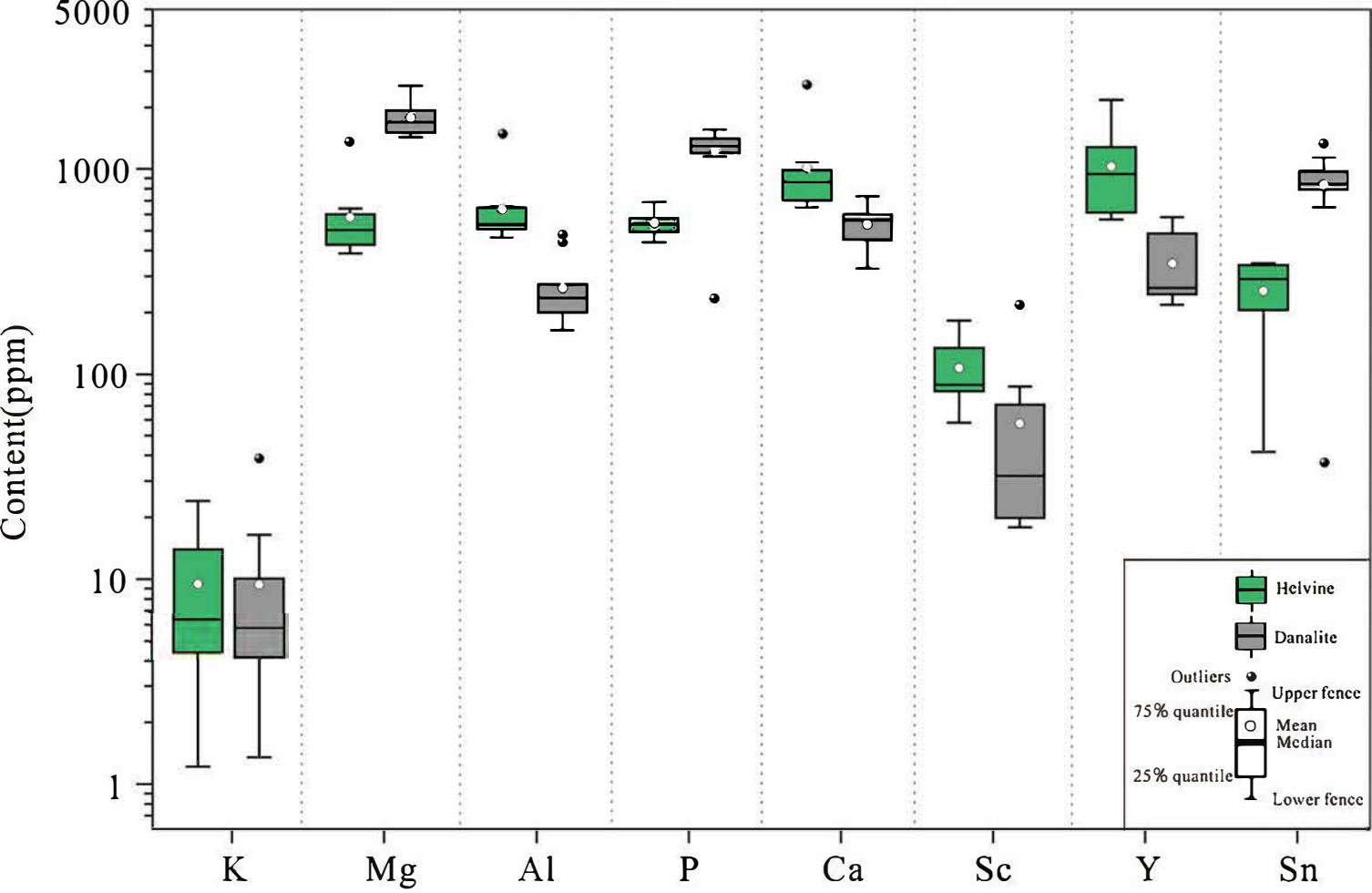
5000
1000
100
10
1
Content(ppm)
K
Mg
Al
P
Ca
Sc
Y
Sn
Helvine
Danalite
Outliers
Upper fence
75% quantile
Mean
Median
25% quantile
Lower fence

Fig 7

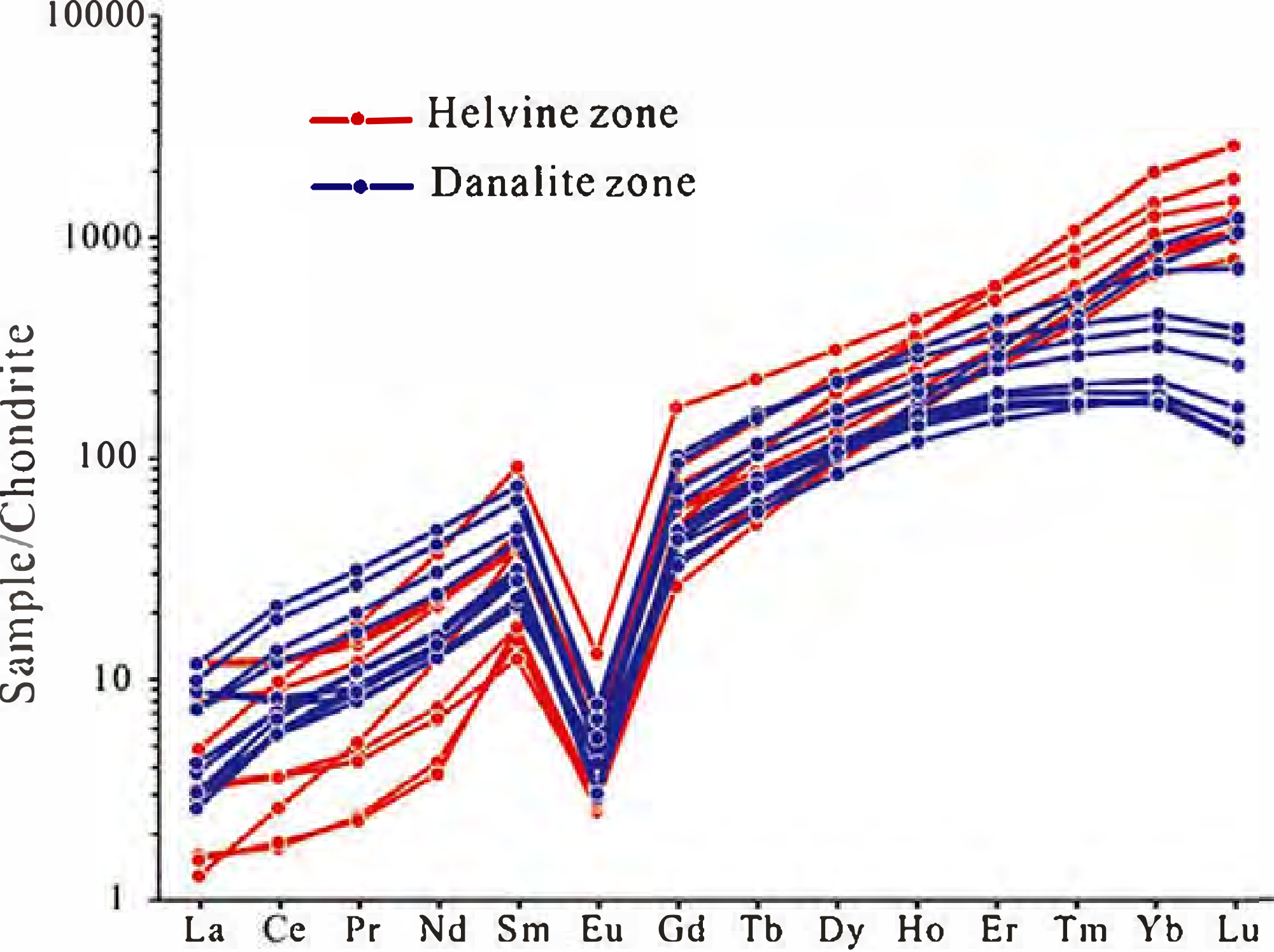
Helvine zone
Danalite zone
Sample/Chondrite
10000
1000
100
10
1
La
Ce
Pr
Nd
Sm
Eu
Gd
Tb
Dy
Ho
Er
Tm
Yb
Lu

Fig 8

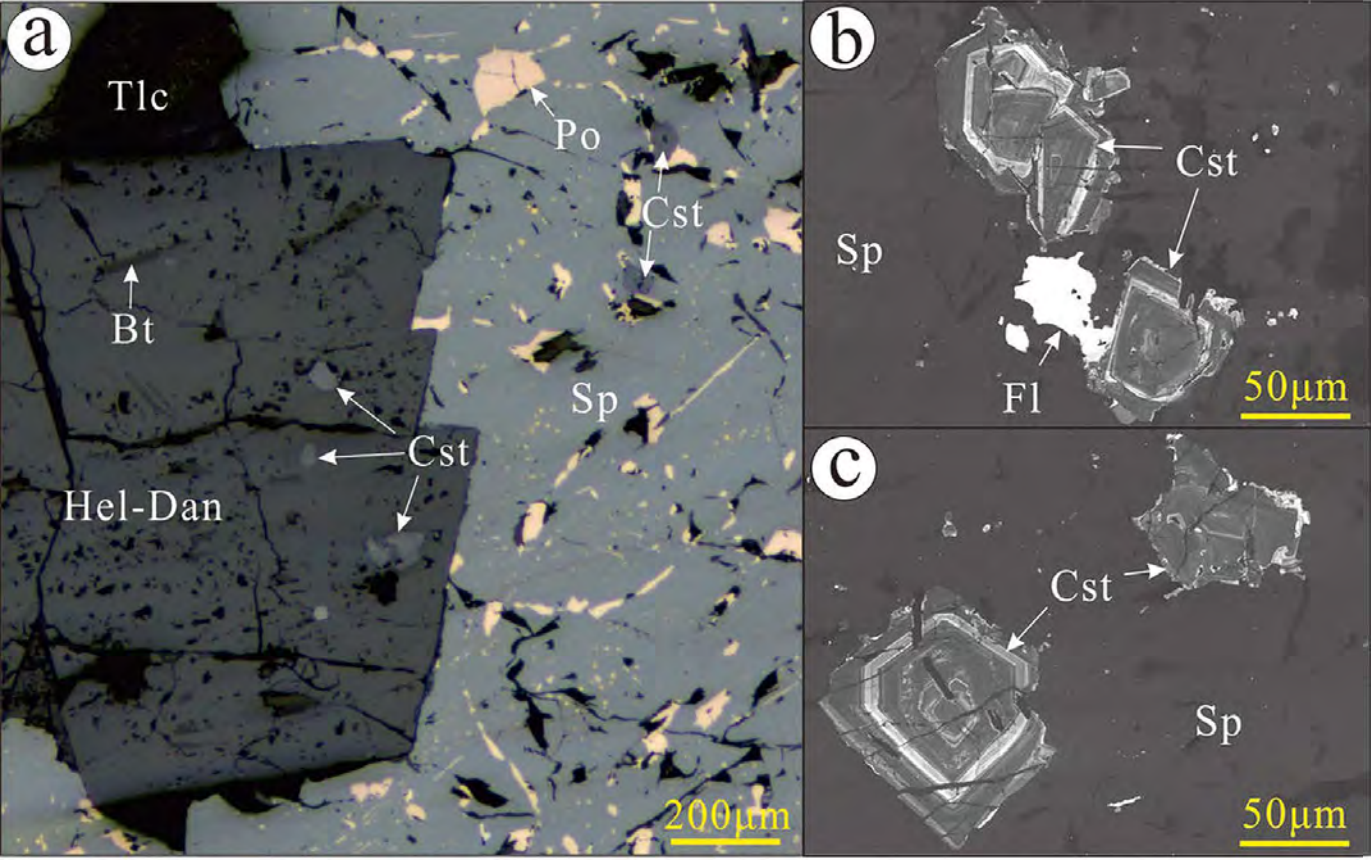

Fig 9

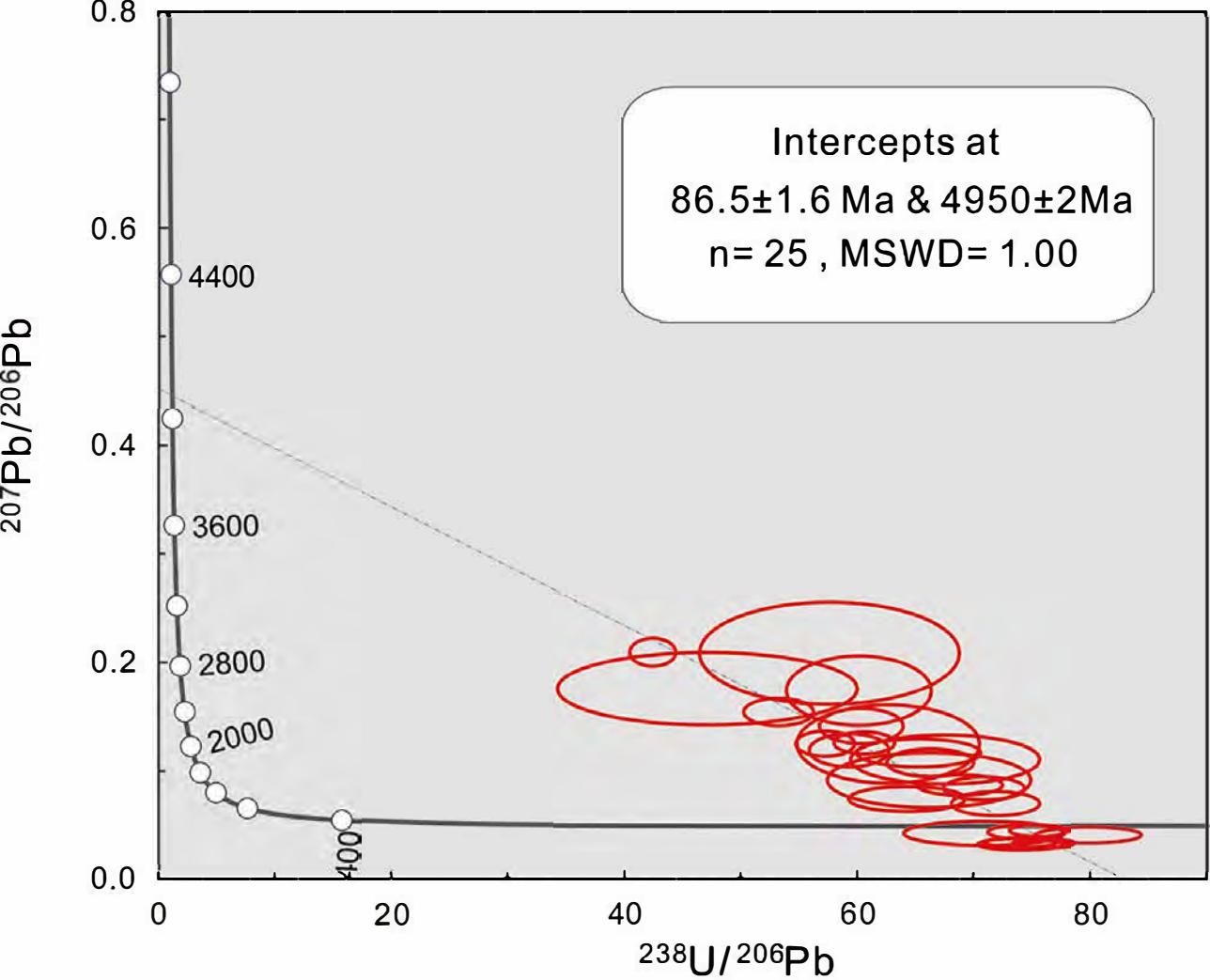
Intercepts at
86.5±1.6 Ma & 4950±2Ma
n= 25 , MSWD= 1.00
4400
3600
2800
2000
400
0.8
0.6
0.4
0.2
0.0
0
20
40
60
80
207Pb/206Pb
238U/206Pb

Fig 10

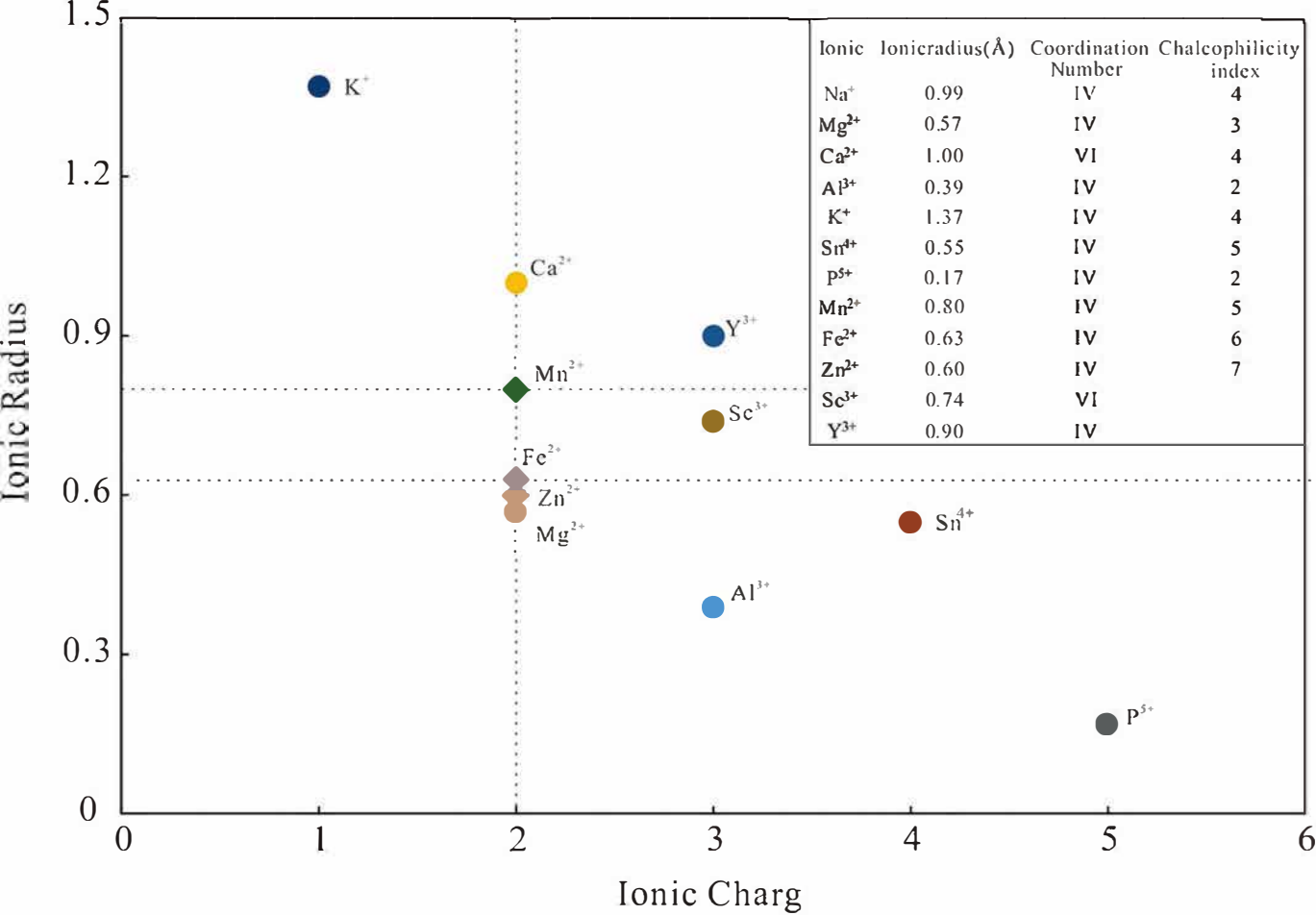

Ionic	Ionicradius(Å)	Coordination Number	Chalcophilicity index
Na^{+}	0.99	IV	4
Mg^{2+}	0.57	IV	3
Ca^{2+}	1.00	VI	4
Al^{3+}	0.39	IV	2
K^{+}	1.37	IV	4
Sn^{4+}	0.55	IV	5
P^{5+}	0.17	IV	2
Mn^{2+}	0.80	IV	5
Fe^{2+}	0.63	IV	6
Zn^{2+}	0.60	IV	7
Sc^{3+}	0.74	VI	
Y^{3+}	0.90	IV	

Fig 11

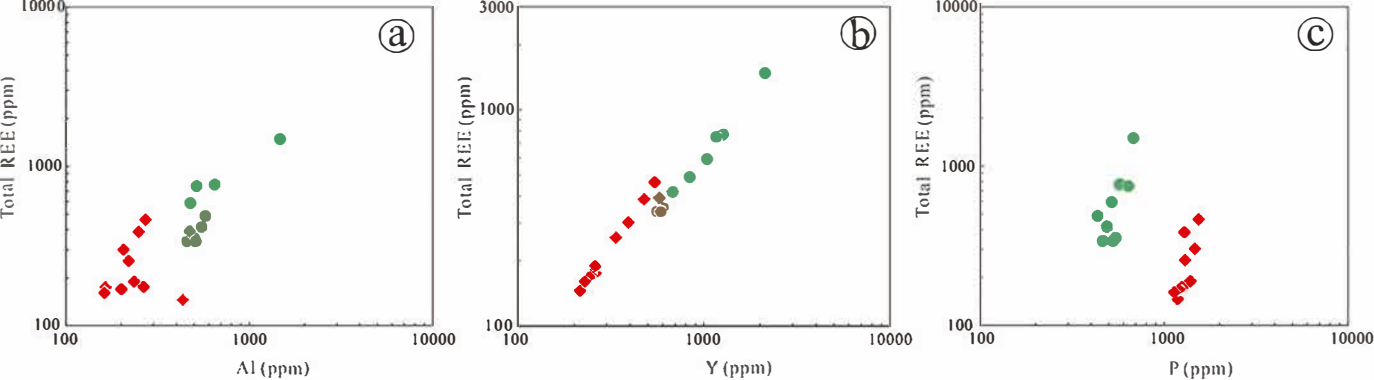
a
Total REE (ppm)
10000
1000
100
100
1000
10000
Al (ppm)
b
Total REE (ppm)
3000
1000
100
100
1000
10000
Y (ppm)
c
Total REE (ppm)
10000
1000
100
100
1000
10000
P (ppm)

Fig 12

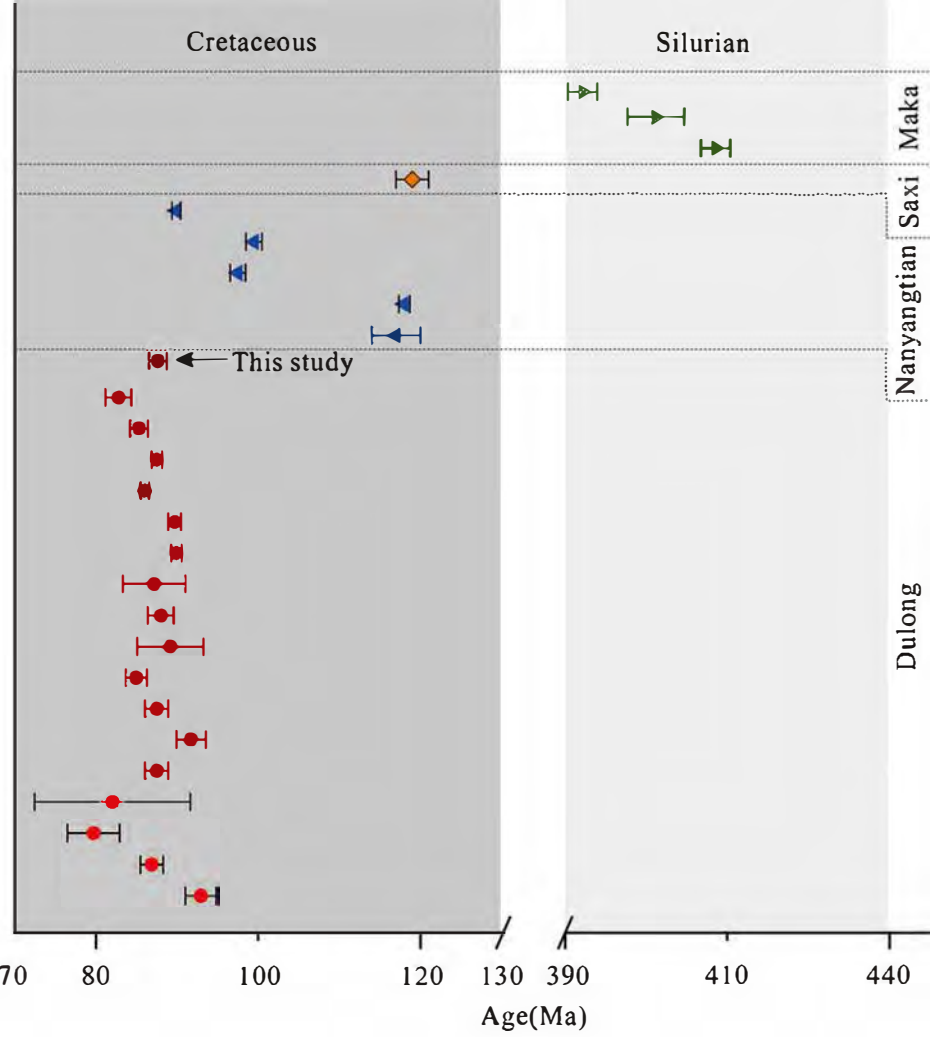
Cretaceous
Silurian
Maka
Saxi
Nanyangtian
Dulong
This study
70
80
100
120
130
390
410
440
Age(Ma)

Fig 13

Table1 Major element compositions of Helvine-Danalite

Locality	Core	a	b	c	d	e	f
Sample	*n*=5	*n*=5	*n*=5	*n*=5	*n*=5	*n*=5	*n*=5
Na_2O(wt.%)	0.13	0.10	0.14	0.19	0.05	0.05	0.07
MgO	0.05	0.03	0.12	0.07	0.32	0.05	0.29
Al_2O_3	0.20	0.20	0.05	0.13	0.01	0.10	0.01
SiO_2	32.78	32.63	32.64	32.67	32.73	32.89	32.75
CaO	0.27	0.25	0.07	0.20	0.00	0.13	0.06
MnO	37.25	38.54	22.87	29.96	11.74	38.70	8.38
FeO	10.97	9.91	23.73	17.14	30.38	9.74	33.68
ZnO	1.71	1.58	3.83	2.85	9.38	1.72	9.21
S	5.77	5.80	5.77	5.83	5.88	5.71	5.82
O≡S	-2.88	-2.90	-2.88	-2.91	-2.93	-2.85	-2.91
**BeO	13.66	13.59	13.60	13.61	13.64	13.70	13.65
Toal	99.91	99.74	99.94	99.76	101.22	99.97	101.01
Cations							
Na(apfu)	0.02	0.02	0.02	0.03	0.01	0.01	0.01
Mg	0.01	0.00	0.02	0.01	0.04	0.01	0.04
Al	0.02	0.02	0.01	0.01	0.00	0.01	0.00
Si	3.00	3.00	3.00	3.00	3.00	3.00	3.00
Ca	0.03	0.02	0.01	0.02	0.00	0.01	0.01
Mn	2.88	3.00	1.78	2.33	0.91	2.98	0.65
Fe	0.84	0.76	1.82	1.31	2.32	0.74	2.57
Zn	0.12	0.11	0.26	0.19	0.64	0.12	0.62
$\sum M$	3.83	3.86	3.86	3.83	3.87	3.84	3.84
S	0.99	1.00	0.99	1.00	1.01	0.98	1.00
Be	3.00	3.00	3.00	3.00	3.00	3.00	3.00
Ternary							
mol.%							

Helvine	75.15	77.56	46.08	60.70	23.52	77.70	16.87
Danalite	21.82	19.66	47.16	34.24	60.01	19.28	66.88
Genthelvite	3.03	2.79	6.76	5.06	16.47	3.02	16.25

n=number of spots.**BeO calculated assuming Si=3 and Be=3.

Table 2 Trace element compositions of Helvine-Danalite (ppm)

	Mg	Al	P	K	Ca	Sc	Y	Sn	La	Ce	Pr	Nd	Sm	Eu	Gd	Tb	Dy	Ho	Er	Tm	Yb	Lu
Helvine-1	390	553	493	-	827	82.7	689	306	3.64	9.56	1.76	13.4	7.47	0.43	15.6	4.13	41.8	14.4	66.5	16.7	187	34.4
Helvine-2	426	507	549	-	706	92.6	612	323	1.03	2.98	0.58	4.48	3.36	0.21	8.68	2.89	33.0	11.8	58.1	15.1	177	34.1
Helvine-3	467	645	568	-	965	182	1277	348	0.49	1.40	0.29	2.54	2.94	0.19	12.6	5.00	62.4	24.3	125	34.8	407	82.8
Helvine-4	459	654	575	-	989	182	1279	344	0.47	1.47	0.28	2.25	3.37	0.20	12.5	4.89	63.3	24.5	126	34.8	413	83.6
Helvine-5	541	581	439	-	1076	84.8	848	205	2.45	7.27	1.46	12.8	8.83	0.51	19.6	5.34	55.1	18.1	81.1	19.4	216	40.4
Helvine-6	603	518	639	-	898	112	1176	87	1.50	7.90	2.15	22.2	17.8	0.96	44.0	10.8	99.8	30.7	125	28.4	299	59.4
Helvine-7	387	481	523	-	698	57.8	1046	42	0.40	2.11	0.63	7.36	7.59	0.42	23.4	6.92	77.2	25.3	109	25.0	261	47.0
Helvine-8	1364	1483	692	4.63	2574	134	2174	272	21.4	76.2	15.4	124	66.1	4.21	119	25.3	210	59.7	222	44.1	420	76.7
Helvine-9	540	462	467	-	742	64.8	566	274	3.70	9.88	1.87	13.9	7.92	0.40	15.1	3.79	36.9	12.3	53.2	12.9	142	25.5
Helvine-10	643	513	528	-	650	82.7	593	340	0.99	2.91	0.52	3.99	2.40	0.21	6.81	2.40	30.3	11.4	56.8	15.0	172	32.1
Danalite-1	1690	477	1234	196	326	87.0	582	37.0	2.71	6.32	0.98	7.43	4.07	0.33	9.04	2.64	32.6	12.9	65.6	17.1	190	39.3
Danalite-2	1490	221	1321	38.0	516	50.1	339	891	2.21	9.48	1.97	14.4	8.17	0.35	16.0	4.88	47.3	14.4	52.7	9.41	66.5	8.51
Danalite-3	2550	438	1200	36.6	629	28.0	218	652	0.97	4.46	0.96	7.43	4.51	0.30	8.42	2.70	27.2	8.51	31.2	5.47	39.1	4.55
Danalite-4	1926	267	1309	14.8	566	18.4	263	838	0.88	4.63	1.13	8.55	5.63	0.22	10.8	3.58	37.0	11.2	39.8	6.44	41.1	4.39
Danalite-5	1425	166	1268	-	490	19.9	249	843	1.16	5.74	1.28	9.81	6.15	0.21	12.3	3.88	37.9	10.9	37.2	5.90	37.5	3.93
Danalite-6	1500	200	1222	19.8	579	17.9	245	793	1.28	5.72	1.31	9.53	5.80	0.23	11.9	3.72	35.4	10.7	36.6	5.80	36.3	3.82
Danalite-7	1706	235	1407	84.2	562	31.9	263	979	0.94	5.28	1.31	9.39	6.08	0.24	12.1	3.85	38.2	11.3	41.5	6.96	46.6	5.44
Danalite-8	1755	207	1487	6.82	603	70.9	397	1134	2.25	10.8	2.42	18.2	9.32	0.39	18.6	5.47	53.6	16.3	60.5	11.1	81.2	11.1
Danalite-9	1591	250	1293	29.5	449	69.6	483	897	3.61	17.2	3.77	28.2	14.5	0.48	26.6	7.53	70.2	20.6	73.8	13.1	93.6	12.4
Danalite-10	1644	164	1152	-	451	21.1	231	843	0.80	4.51	1.06	8.52	5.42	0.22	11.0	3.53	34.2	10.0	35.1	5.67	36.6	3.90
Danalite-11	2337	273	1552	-	738	218	552	1326	3.04	14.9	3.25	24.3	12.4	0.56	24.4	7.16	71.1	22.4	88.9	17.7	148	23.2

“-” means under the detection limit.

Table 3 LA-ICP-MS U–Pb dating results of cassiterite from the Dulong Tin-Zinc polymetallic deposit.

Spots	Common Pb (ppm)	Total Pb (ppm)	^{232}Th (ppm)	^{238}U (ppm)	Isotopic Ratios						Isotopic Age (Ma)	
					$^{207}Pb/^{206}Pb$	1σ	$^{207}Pb/^{235}U$	1σ	$^{206}Pb/^{238}U$	1σ	$^{206}Pb/^{238}U$	1σ
DL741	0.13	0.24	0.03	18.36	0.03569	0.00340	0.05985	0.00509	0.01317	0.00031	84.4	2.0
DL74-2	0.16	0.00	0.00	0.27	0.02537	0.00960	0.49927	0.09788	0.01738	0.00222	111	14.1
DL74-3	0.00	0.13	0.00	10.14	0.04241	0.00624	0.06987	0.00883	0.01254	0.00047	80.3	3.0
DL74-4	0.09	0.15	0.00	11.31	0.03666	0.00400	0.06343	0.00575	0.01352	0.00037	86.6	2.3
DL74-5	0.00	0.16	0.04	10.44	0.08023	0.01006	0.13394	0.01482	0.01393	0.00048	89.2	3.1
DL74-6	0.16	0.18	0.03	13.10	0.04754	0.00449	0.08203	0.00661	0.01325	0.00029	84.8	1.8
DL74-7	0.28	0.02	0.00	0.88	0.08124	0.01933	0.27456	0.05713	0.01598	0.00132	102	8.4
DL74-8	0.40	0.20	0.05	14.20	0.04677	0.00538	0.08059	0.00824	0.01345	0.00038	86.1	2.4
DL74-9	0.13	0.01	0.00	0.81	0.08087	0.01815	0.22557	0.03523	0.01482	0.00118	94.8	7.5
DL74-10	0.16	0.05	0.00	2.32	0.11549	0.02015	0.15919	0.01816	0.01558	0.00080	99.6	5.1
DL74-11	0.19	0.21	0.01	8.66	0.13627	0.01028	0.28645	0.01715	0.01652	0.00047	106	3.0
DL74-12	0.11	0.13	0.02	5.17	0.12906	0.01325	0.27687	0.02562	0.01688	0.00064	108	4.1
DL74-13	0.43	0.16	0.02	5.54	0.15082	0.01726	0.30155	0.02038	0.01749	0.00051	112	3.2

DL74-14	0.11	0.10	0.02	4.90	0.12520	0.01550	0.22407	0.01938	0.01511	0.00056	96.7	3.6
DL74-15	0.26	0.11	0.01	3.92	0.20544	0.02705	0.32296	0.02749	0.01659	0.00065	106	4.1
DL74-16	0.15	0.12	0.01	6.33	0.10164	0.01016	0.17451	0.01384	0.01455	0.00051	93.1	3.3
DL74-17	0.00	0.05	0.01	2.25	0.13674	0.01737	0.24638	0.02237	0.01534	0.00083	98.1	5.2
DL74-18	0.13	0.28	0.07	15.05	0.08556	0.00858	0.16329	0.01463	0.01412	0.00046	90.4	2.9
DL74-19	0.21	0.17	0.02	4.74	0.18050	0.01539	0.39962	0.02615	0.01881	0.00070	120	4.4
DL74-20	0.31	0.04	0.02	2.73	0.05885	0.01548	0.08272	0.01535	0.01412	0.00091	90.4	5.8
DL74-21	0.72	0.37	0.02	7.11	0.23255	0.01461	0.68060	0.03474	0.02359	0.00073	150	4.6
DL74-22	0.37	0.01	0.00	0.66	0.05627	0.01506	0.19074	0.03857	0.01513	0.00132	96.8	8.4
DL74-23	0.18	0.01	0.00	0.20	0.02620	0.01152	0.51409	0.11291	0.02124	0.00383	135	24.2
DL74-24	0.00	0.02	0.03	0.96	0.14262	0.02802	0.39899	0.05537	0.01665	0.00114	106	7.2
DL74-25	0.43	0.21	0.00	15.28	0.03955	0.00581	0.06027	0.00682	0.01353	0.00044	86.6	2.8